IMPLEMENTATION OF A NOVEL FLUORESCENT HUNTINGTON'S DISEASE MODEL AND BRANAPLAM TO STUDY THE INTERACTION BETWEEN HUNTINGTIN AND HAP40

IMPLEMENTATION OF A NOVEL FLUORESCENT HUNTINGTON'S DISEASE MODEL AND BRANAPLAM TO STUDY THE INTERACTION BETWEEN HUNTINGTIN AND HAP40

BY NOLA BEGEJA, B.Sc.

A Thesis Submitted to the School of Graduate Studies in Partial Fulfillment of the Requirements for the Degree Master of Science

McMaster University MASTER OF SCIENCE (2021)

Hamilton, Ontario

Biochemistry and Biomedical Sciences

Title: Implementation of novel fluorescent Huntington's disease model and branaplam to study the interaction between huntingtin and HAP40

Author: Nola Begeja, B.Sc

Supervisor: Dr. Ray Truant

Number of Pages: xi, 79

ABSTRACT

Huntington's disease (HD) is a neurodegenerative disease caused by a CAG expansion in the *HTT* gene, which causes an expansion in the polyglutamine tract of the huntingtin protein. In 2018, the cryo-EM structure of the 350 kDa protein huntingtin (Htt) in complex with huntingtin associated protein of 40 kDa (HAP40) was solved, which demonstrated that huntingtin had to be co-translated and complexed with HAP40 to retain structure. However, little is known about HAP40 and thus the biological relevance of this structure. In this project, we transduced cells with fluorescently labelled recombinant apo-Htt or Htt-HAP40 to determine if HAP40 must be complexed with huntingtin in order for huntingtin to have biological activity. This method has not been implemented in HD research and may also improve current fluorescent microscopy models for huntingtin, as it has the advantage of looking at full-length protein rather than small fragments. We also found that with the huntingtin lowering drug branaplam, there is a linear correlation between huntingtin and HAP40 levels, where HAP40 levels will decrease when huntingtin levels are directly decreased as detected by western blot analysis. Furthermore, we found that this lowering effect by branaplam ameliorates DNA repair deficits in HD. With the potential for branaplam to become a treatment for HD, we should continue to test its effect on other HD-associated phenotypes to determine the effect of huntingtin and downstream HAP40 lowering.

Acknowledgements

I would like to thank my supervisor Dr. Ray Truant for hiring me to work in his lab when I was only in the third year of my undergraduate program without any prior lab experience. Thank you for taking a chance on me and providing me with support throughout the following years, encouraging me to keep going when experiments went wrong, and believing in me and my scientific abilities. I would also like to thank my committee members Dr. Sara Andres and Dr. Jose Moran Mirabal for all of your insights and ideas on how to approach problems, and your encouragement throughout the past two years. I would also like to thank Dr. Rachel Harding and the Arrowsmith lab for their collaborations with our lab and doing the hardest part of this project which was protein purification of an unfriendly protein.

I would also like to thank all the members in the Truant lab for being lovely people to work with. Thank you Dr. Tam Maiuri, Dr. Claudia Hung, Carlos Barba Bazan, Celeste Suart, Natasha Savic, Christina Peng, Katie Neuman and Siobhan Goss for creating a positive lab environment. I would especially like to thank Claudia for all her help during her time in the lab - you were so patient with me when teaching me new experiments, you always genuinely cared for my success in the lab and my overall wellbeing, you mentored me and helped troubleshoot my experiments even after you moved on from the lab to your career.

Last but not least, I would like to thank my friends and family for their support and encouragement. Thank you to my parents and Emma for always checking up on me and being there for me whenever things got rough, thank you to my friends who helped me forget about stressful experiments going wrong, and a very big thank you to my boyfriend David who is my number one supporter and fan. I am so lucky to have someone who has never left my side and has been so accommodating and loving, for you I am so grateful.

Table of Contents

Abbreviations

8-OHdG	8-hydroxy-2' -deoxyguanosine
8-oxo-G	8-hydroxyguanine
AD	Alzheimer's Disease
AF488	Alexa Fluor 488
AF488-apo-Htt	AF488 labelled recombinant apo huntingtin with 23 glutamines
AF488-Htt-HAP40	AF488 labelled recombinant HAP40 complexed huntingtin with 23 glutamines
ANOVA	analysis of variance
ASO	antisense oligonucleotide
ATP	adenosine triphosphate
BACHD	bacterial artificial chromosome Huntington's Disease mouse
BBB	blood brain barrier
BDNF	brain derived neurotrophic factor
BER	base excision repair
CAG	cytosine adenine guanine
CBP	CREB binding protein
CNS	central nervous system
CREB	cyclic AMP response element-binding protein
Cryo-EM	cryo-electron microscopy
DDR	DNA damage response
DMSO	dimethyl sulfoxide
DNA	deoxyribonucleic acid
DSB	double stranded DNA break
ER	endoplasmic reticulum
F8A	Factor 8 associated gene
FLIM	fluorescence lifetime imaging microscopy
FP	fluorescent protein
FRET	Förster resonance energy transfer
GWAS	genome wide association study
H2B	histone 2B
HAP40	huntingtin associated protein of 40 kDa
HD	Huntington's Disease
HEAT (repeat)	huntingtin, elongation factor 3, protein phosphatase 2A and lipid kinase TOR
HEPES	4-(2-hydroxyethyl)-1-piperazineethanesulfonic acid
hTERT	human telomerase reverse transcriptase
HTT	huntingtin gene
Htt	huntingtin protein
IDR	intrinsically disordered region
iPSC	induced pluripotent stem cell

MW	molecular weight
MWCO	molecular weight cut-off
N17	Amino (N) terminal 17 amino acids of huntingtin
NES	nuclear export signal
NLS	nuclear localization signal
p53	tumor protein 53
PAR	poly ADP-ribose
PARP1	poly ADP-ribose polymerase 1
PBS	phosphate-buffered saline
PD	Parkinson's Disease
Phospho-N17	phosphorylated serine residues 13 and 16 of the N-terminal 17 amino acids of huntingtin
POI	protein of interest
PTM	post-translational modification
PVDF	polyvinylidene fluoride
RNA	ribonucleic acid
ROS	reactive oxygen species
ROS	reactive oxygen species
RPE1	retinal pigmented epithelial 1
SEC	size exclusion chromatography
shRNA	small hairpin ribonucleic acid
siRNA	small interfering ribonucleic acid
SMA	spinal muscular atrophy
SNP	single nucleotide polymorphism
TBS-T	tris-buffered saline with 0.1% Tween 20
TCEP	tris(2-carboxyethyl)phosphine
TFP	tetrafluorophenyl ester
TruHD Q21Q18	hTERT immortalized spousal control fibroblasts with glutamine lengths of 21 and 18
TruHD Q43Q17	hTERT immortalized heterozygous HD patient derived fibroblasts with glutamine lengths of 43 and 17
XRCC1	X-ray repair cross-complementing protein 1
YFP	yellow fluorescent protein
γH2AX	phosphorylated histone 2A

Table of Figures

Declaration of Academic Achievement

Nola Begeja performed all the experiments and data analysis except for the γH2AX fluorescence intensity measurement in branaplam treated cells (Fig. 10D) which was done by Carlos Barba Bazan.

Chapter 1: Introduction

1.1 Overview of Huntington's Disease

Huntington's disease is a neurodegenerative disease inherited in an autosomal dominant fashion.[1] It affects an estimated 10.6 individuals per 100,000 in Europe and North America but has a lower prevalence or rate of diagnosis in certain geographic regions, such as Asia, where only 1 in every 100,000 people is affected.[2] The age of symptom onset can be highly variable but averages 40 years, with a life expectancy of 15-20 years after symptoms first appear. Symptoms of HD can be categorized into the clinical triad of psychiatric illness like depression and anxiety, cognitive impairments, and disordered movement such as involuntary, jerky movements.

The cause of death in individuals with HD is typically due to secondary complications arising from these symptoms. For example, disordered motor control can cause difficulty in swallowing, which can lead to choking or aspiration pneumonia, two of the most common causes of death in HD. Another common cause of death in HD is cardiac failure, which indicates that multiple organ systems are affected by the disease, although predominantly affecting the brain. In the brain, the disease pathology begins with gradual atrophy of the medium-sized projection spiny neurons of the striatum. It eventually also progresses to the atrophy of other brain structures, such as the cerebral cortex.[3] Although the disease is age onset and neuronal atrophy is not seen until adult ages, neurological changes occur as early as the age of four.[4]

1.2 Genetic cause of the disease

HD is caused by a CAG trinucleotide repeat expansion in the *HTT* gene of the short arm of chromosome 4 which translates to a polyglutamine tract expansion in the huntingtin protein, often referred to as "mutant" huntingtin.[5] Healthy individuals have 35 or fewer CAG repeats in

the *HTT* gene, but full penetrance of the disease occurs with 40 or more repeats. Individuals with 36-39 repeats may or may not develop a milder form of HD.[6,7] The age of symptom onset has an inverse correlation with the number of CAG repeats in the *HTT* gene, meaning that a higher number of repeats leads to earlier disease onset.[8] The median number of CAG repeats in adult-onset HD is 43, while repeats of over 55 usually result in early-onset Juvenile HD.[9] However, there is a lot of variation in age of onset between adults with the same repeat lengths.[10] Genome-wide association studies (GWAS) have discovered single nucleotide polymorphisms (SNP's) in genes that influence this variability in age onset aside from CAG length, with some being within the *HTT* gene, such as CAA interruptions within the CAG tract.[10–12]

1.3 Oxidative stress in HD and other neurodegenerative diseases

Various neurodegenerative diseases like Alzheimer's disease (AD) and Parkinson's disease (PD) share similarities with HD in terms of progressive neuronal loss and symptoms of impaired cognitive and motor function. Additionally, compared to healthy individuals of the same age, there is higher oxidative stress in the brains of individuals with neurodegenerative disease.[13–15] Oxidative stress is induced by reactive oxygen species (ROS) which can be produced endogenously in the body or can come exogenously from environmental toxins. Mitochondria are the largest producers of ROS in the body due to the production of $O_2^{\bullet -}$, primarily from the enzyme Complex I in the electron transport chain. Since the brain is one of the most metabolically active organs, it has a high oxygen demand (20% of the body's oxygen consumption) to meet ATP requirements, thus producing high levels of ROS as a by-product.[15]

ROS can damage macromolecules such as DNA and lipids, and with age this damage can accumulate to result in reduced efficiency in repair and energy production, and even cell death.[16] Since neurons are postmitotic, they must fix DNA lesions by non-replication based DNA repair

methods such as the base excision repair (BER) pathway. Moreover, neuronal loss is extremely detrimental because neural progenitor cells are very limited in their ability to divide and differentiate. The most common ROS-induced DNA lesion is the hydroxylation of the C-8 residue in guanine to form 8-oxoguanine (8-oxo-G) or 8-oxo-2'-deoxyguanosine (8-OHdG). The 8-OHdG residue is used as a biomarker of oxidative damage; it has been found in HD post-mortem brain tissue of the caudate and in leukocytes obtained from the sera of HD patients.[17,18]

1.4 DNA damage in HD as a driver of disease pathology

Other forms of DNA damage are also elevated in various HD mouse and cell models as well as HD patient tissue samples, such as post-mortem brain tissue, peripheral blood mononuclear cells, and fibroblasts.[19–21] The CAG trinucleotide repeat found in the *HTT* gene is also genetically unstable and prone to somatic expansion if it is already elongated, such as in HD.[22–25] This is especially prevalent in the neurons of post-mortem brain tissue, where up to 1,000 repeats are found in some cells of the striatum and cortex.[26] Moreover, a 2015 genome wide association study (GWAS) found that SNPs in five different DNA repair genes significantly contribute to variation in age onset. When Pathway Analysis was conducted in this GWAS by clustering all the SNP data by function and pathway, regardless of statistical significance, the researchers found that the most significant pathways involved in altering disease age onset were DNA repair, followed by mitochondrial fission and oxidoreductase activity.[27] This suggests that improper DNA damage repair could exacerbate disease, therefore it may be a driver of pathology.

Aside from the involvement of well characterized DNA repair genes and proteins in HD pathology, there is also evidence that the HD-implicated huntingtin protein is involved in the DNA damage response (DDR). Maiuri *et al.* from the Truant lab have demonstrated that under

oxidative stress, huntingtin interacts with BER DNA repair proteins like X-ray repair cross-complementing protein 1 (XRCC1) and poly ADP-ribose polymerase 1 (PARP1). Interestingly, there is evidence that PARP1 inhibitors can improve symptoms in HD mice.[28] PARP1 is an enzyme which catalyzes the polymerization of poly ADP-ribose (PAR) chains on other DNA repair enzymes to recruit them to the site of damage (a process known as PARylation).[29] Unpublished data from our lab has found that huntingtin interacts with PAR chains non-covalently, and that HD fibroblasts have higher levels of PAR chains formed in response to DNA damage compared to controls.[30]

Other evidence that huntingtin is involved in the DDR was found through a microscope laser micro-irradiation assay, where phosphorylated huntingtin was recruited to the site of DNA damage. This assay induces a variety of DNA damage including strand breaks and base lesions at the area or stripe of interest to investigate the recruitment of DDR proteins.[31] In HD patient derived fibroblasts, mutant huntingtin protein could still be recruited to sites of damage, suggesting that elevated DNA damage is not due to a loss of function of huntingtin recruitment in the DNA damage response.

This recruitment is also dependent on activation of ataxia telangiectasia mutated (ATM), a serine/threonine protein kinase which is activated by various forms of DNA damage to phosphorylate other proteins, leading to the initiation of DNA damage checkpoints.[32,33] In HD induced pluripotent stem cells (iPSCs) and HD bacterial artificial chromosome transgenic mice (BACHD), ATM inhibition or depletion reduced cell death and improved behavioural deficits.[34] Since huntingtin requires ATM for recruitment, the mechanism behind symptom amelioration could be because of the downstream inhibition of huntingtin recruitment, which would suggest a detrimental effect of mutant huntingtin on DNA. This detrimental effect of mutant huntingtin

was suggested by Enokido *et. al* who found that mutant huntingtin aberrantly interacts with the DNA repair protein Ku70 which prevents DNA double stranded break (DSB) repair and results in more DNA damage.[35] Furthermore, Gao *et. al* found that huntingtin has a role in transcription coupled DNA repair, but mutant huntingtin reduces the activity of the repair complex resulting in DNA damage accumulation.[36]

1.5 Huntingtin Protein

Huntingtin is a large protein with a molecular mass of 350 kDa made up of 3144 amino acids. It is ubiquitously expressed in humans but has the highest level of expression in neurons of the central nervous system.[37] Huntingtin is found in metazoans and is highly conserved among vertebrates. Exon 1 of huntingtin is comprised of the N17 domain (first 17 amino acids), followed by a polyglutamine tract which is expanded in HD, and a polyproline stretch.[10] Much of the protein is comprised of α-helices that arrange to form HEAT (huntingtin, elongation factor 3, protein phosphatase 2A and lipid kinase TOR) repeats.[38] HEAT repeats typically form solenoid structures and can undergo elastic conformational changes upon the binding of other proteins and can serve as a scaffold for multivalent protein interaction.[39] HEAT repeats can be found in all orthologs of huntingtin, and are very similar in terms of distribution, number, and sequence similarity. The N17 domain and polyglutamine tract (at least 4 glutamines) are highly conserved in vertebrates, with the number of glutamines in the polyglutamine tract increasing with higher species. Humans have the longest known polyglutamine tract.[40]

1.5.1 Cellular localization of huntingtin

Huntingtin is localized to the cytoplasm, nucleus, microtubules, perinuclear space, and found in organelles like the endoplasmic reticulum (ER), Golgi apparatus, and mitochondria.[39,41,42] These localizations are regulated by post-translational modifications

(PTM's). For example, methionine 8 in the N17 domain is thought to act as a ROS sensor because when sulphoxidized, it triggers the release of huntingtin from the ER.[43] This change promotes the phosphorylation of serine residues 13 and 16 (S13/S16) which promotes the retention of the protein in the nucleus.[44,45] In HD models, S13/S16 is hypo-phosphorylated, and treatments that increase this phosphorylation have shown therapeutic effects.[45,46]

Huntingtin contains a proline-tyrosine nuclear localization signal (PY-NLS) at amino acids 174-207 which allows for nuclear entry using the karyopherin β1/ β2 pathway. It also contains two nuclear export signals (NES) which are found within the N17 domain and the other close to the carboxyl terminus at amino acids 2364-2414.[47]

1.5.2 Aggregation of huntingtin

Aside from oxidative stress, another commonality in neurodegenerative diseases is the aggregation and accumulation of protein, which some consider to be the cause of brain damage and cellular dysfunction.[48] In Alzheimer's, β-amyloid peptides form intracellular plaques in the brain which is widely thought to be a driver of pathology, however many clinical trials with drugs designed to clear these plaques have been unsuccessful, or in some cases have even worsened disease progression.[49,50] In HD, this theory was developed when intranuclear inclusions of fragmented huntingtin protein were found in post-mortem HD cortex and striatum, and the extent of huntingtin accumulation was correlated to the CAG length of the patients *HTT* gene.[51] While in some mouse HD models these aggregates correlate with the susceptibility to cell death and stage of disease, other studies have suggested that these aggregates may be protective and increase cell life span as they sequester fragmented mutant huntingtin to prevent solubilization of the protein and interaction with other proteins.[52,53] Protein aggregation could

also be a downstream effect of a pathological mechanism, as in some models increased DNA damage is found prior to the formation of protein aggregates.[54]

1.5.3 Cellular functions of huntingtin

Huntingtin is estimated to interact with over 350 cellular proteins and is also found to associate with other cellular components like DNA, RNA, and lipids.[10,42] This wide variety of interactions is reflected in the vast range of cellular functions the protein is involved in. Huntingtin is required for proper embryonic development; one gene copy is sufficient, however reducing protein levels under 50% disrupts the formation of the central nervous system (CNS).[55,56] Moreover, the protein has critical roles in neurons for synaptic transmission as it can transport synaptic precursor vesicles and brain-derived neurotrophic factor (BDNF)-containing vesicles to the synapse.[57] In other cell types including the axons of neurons, huntingtin is involved in anterograde and retrograde vesicular transport of a variety of cargo, including organelles. It also participates in endosomal trafficking and vesicle recycling, where it interacts with huntingtin associated protein of 40 kDa (HAP40).[58]

Huntingtin also has a role in responding to cell stress, which is evident by the multiple tumour protein 53 (p53) responsive elements (RE's) found in the *HTT* gene.[59,60] p53 has an essential role of conveying stress signals in the cell and acts as a tumor suppressor. During stress like cold temperature shock or γ-irradiation, p53 binds to these RE's to increase transcription of *HTT* mRNA and ultimately huntingtin levels.[59] Additionally, huntingtin responds to heat shock once the S13/S16 residues are phosphorylated. This triggers nuclear retention where it transcriptionally regulates other stress response proteins and associates with stress-dependent cofilin-actin rods to prevent actin treadmilling.[61] The phosphorylation of S13/S16 is also

important for huntingtin to respond to DNA damage or oxidative stress, as discussed in section 1.4.

Additionally, huntingtin is also involved in transcriptional regulation when the cell is not stressed. Wildtype huntingtin binds to several transcription factors such as cAMP-response element binding (CREB)-binding protein (CBP) and p53.[39,62] However, mutant huntingtin can disrupt the interaction of many transcription factors, resulting in a dysregulated transcriptome.[63,64]

Huntingtin is also required for proper cell division and cell fate determination in progenitor cells. Depleting huntingtin results in inappropriate assembly and orientation of the mitotic spindle, which causes a high level of cell apoptosis following mitosis. During mitosis, huntingtin localizes to spindle poles and fibers, in addition to general cytoplasmic area outside of the chromosomes.[65]

1.5.4 Structure of Huntingtin

In 2018, the cryo-electron microscope (cryo-EM) structure of huntingtin was solved by purifying recombinant huntingtin in complex with huntingtin-associated protein 40 (HAP40).[38] Purified apo-huntingtin contained too much conformational heterogeneity that prevented cryo-EM analysis. However, a recent 2021 paper by Harding et al. found a low 12 Å resolution structure of apo-huntingtin with a similar general structure as the huntingtin-HAP40 complex.[66] It contained a central cavity where HAP40 would be found in the complexed structure, suggesting that HAP40 helps retain the structure of huntingtin without altering the general shape. The rest of the structured protein is categorized into N-HEAT and C-HEAT domains (at N- and C-termini) and a “bridge” domain which connects these HEAT repeats (Fig. 1).[66]

About 25% of the model consists of unsolved flexible structures, with the largest unsolved area being the intrinsically disordered region (residues 407-665); a region that hosts multiple phosphorylation sites which modulate protein-protein interactions and accessibility to proteases.[38,67] Exon 1 also has no structure and can take on a wide range of conformational space given the environment that the protein is in.[66] The structured regions of huntingtin do not change with an expanded polyglutamine tract, however expanded exon 1 does cause a conformational change in the intrinsically disordered domain (IDR), and interacts with the C-HEAT domain which is not observed in shorter polyglutamine tracts. [66]

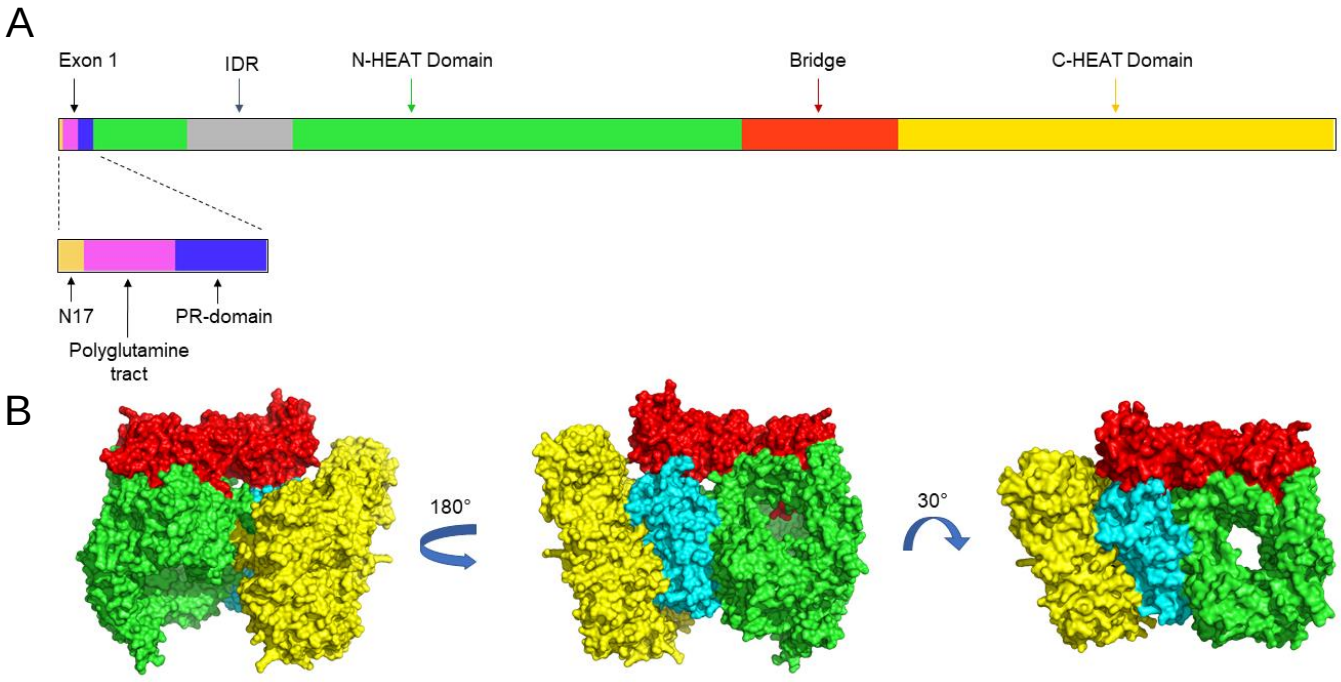

Figure 1: *The structure of the huntingtin protein.* (A) a to-scale representation of full-length huntingtin (3144 amino acids). Exon 1 is made up of the N17 domain, the polyglutamine tract which ranges in length, but is 36+ repeats in HD, and the proline rich domain. Other large areas are colour coded to match the (B) cryo-EM structure (PDB ID: 6X09). The intrinsically disordered domain (IDR) in gray and exon1 are not found on the structure due to high flexibility. On the 3D structure, HAP40 is shown in cyan with high areas of contact with N- and C-HEAT domains; very little of HAP40 can be seen at the back of the structure (left). Bridge domain (red) has points of contact with both HEAT domains and HAP40.

1.6 Huntingtin associated protein of 40 kDa (HAP40)

The gene which codes for HAP40 is considered a "nested" gene as it is found on the X chromosome in an intronic sequence (intron 22) of the Coagulation Factor VIII gene, thus giving the name F8A for Factor 8 associated. In humans, there are three copies of this gene (intron homologous region 1, 2, and 3) where 2 and 3 are located closer to the Xq telomere. All three contribute to the overall HAP40 protein levels.[68–70] Although the gene is associated with coagulation factor VIII, there is no evidence that HAP40 has a role in blood clotting. However, an inversion of intron 22, the sequence which codes for HAP40, leads to hemophilia A, a recessive X-linked coagulation disorder.[71]

Like huntingtin, HAP40 is ubiquitously expressed.[70] However, a single study showed that in primary fibroblasts from HD patients, HAP40 protein levels are highly elevated compared to healthy controls. The same trend is also seen in striatal tissue from HD human post-mortem brains. Not much is known about the function of HAP40 protein other than its role in vesicular trafficking of early endosomes through its interaction with Rab5, a regulatory guanosine triphosphatase (GTPase). HAP40 is also required for huntingtin to join this complex. Once the Rab5-HAP40-huntingtin complex is formed, it regulates the dynamics of early endosome by switching the binding of the endosome from microtubules to actin. Endosomes move along actin for short-range movements but require microtubules for long-range bidirectional movements. Transgenic overexpression of HAP40 limits the velocity and range of movements for these endosomes as it causes detachment of the endosomes from microtubules to switch to actin. This is also apparent in HD cells, where HAP40 is elevated.[58] Overexpression of HAP40 also results in an interaction of it with the N17 domain of huntingtin, which could be pathological as the N17 domain is important for proper protein localization and ROS sensing.[72]

Research in evolutionary biology using bioinformatics has shown that huntingtin and HAP40 most likely co-evolved at the root of eukaryotes due to their co-presence in unikonts (eukaryotic supergroup) but absence in fungi.[73] The interaction between the two proteins is also conserved, proposing the idea that these two proteins are dependent on one another. The cryo-EM structure of huntingtin suggests that this dependence may be for stabilizing structure.[38,67] Although the huntingtin structure could not be solved without being in complex with HAP40 due to its flexible nature, the low-resolution structure of apo-huntingtin still has the same general shape as complexed huntingtin, with a cavity where HAP40 would be found.[66]

Another experiment by Harding et al. showed that when using native top-down mass spectrometry to dissociate the huntingtin-HAP40 complex, the backbone of huntingtin dissociates into C- and N-terminus fragments, but the HAP40 protein stays intact. This type of experiment is done to cause dissociation of non-covalent complexes into their individual subunits. However, the non-covalent interaction between HAP40 and huntingtin is stronger than the covalent bonds between the amino acids of huntingtin. In buffers varying widely in salt concentrations and ranges of pH, the recombinant huntingtin-HAP40 complex remains stable. This very strong interaction between the two proteins is mostly mediated by hydrophobic interactions along the large area of shared interface. Other strong interactions between the two involve a charge-based interaction between the bridge domain of huntingtin and C-terminus end of HAP40. [66]

1.7 HD mouse models

Due to the monogenetic nature of HD, studying the disease using animal models or cell models can be more straightforward than diseases caused by multiple factors. However, many models discredit the importance of the full HTT gene or huntingtin protein by developing

transgenic overexpression models with only small portions of the gene. To develop therapeutics in HD, pre-clinical trials need to be done in animal models to assess safety and efficacy before proceeding to human clinical trials. Unfortunately, drug treatments which are successful in HD mice or animal models have not translated to success in clinical trials, which could be due to a lack of a model that accurately mimics human disease.[74]

The R6/2 mouse is a commonly used transgenic model due to their rapid disease progression which makes them easier to study. They express truncated huntingtin exon 1 with a polyglutamine expansion of 82, along with the wildtype murine homolog of huntingtin. These fragments aggregate in the mouse brain and result in neuronal toxicity.[75,76]

Transgenic full length huntingtin mouse models include the BACHD mouse (generated with bacterial artificial chromosomes) and the YAC (yeast artificial chromosome) mouse, with full genomic human HTT. These have 97 and 125 CAG repeats, respectively. Disease progression in these mice is more like human HD, as they experience progressive and later age onset cognitive and motor symptoms, and selective neurodegeneration of the striatum and cortex.[77,78] However, in all mouse models, the CAG expansion is very high and not representative of most CAG expansion lengths found in human HD.[9]

1.8 HD human cell models

Primary cells derived from human HD patients are a biologically relevant model as they have relevant CAG lengths and contain any epigenetic or cellular changes that occurred during the slow progression of the disease. Neurons, the main cell type implicated in HD, cannot be safely collected from patients. However, fibroblasts can be obtained through a skin biopsy and can be cultured and propagated. Hung et. al immortalized patient fibroblasts using human telomerase reverse transcriptase (hTERT) to create the TruHD cell line, which are commonly

used in the Truant lab. This model overcomes caveats of primary fibroblasts which reach senescence quickly and accumulate chromosomal abnormalities when passaging.[46] The use of hTERT makes this cell line more robust and maintains the function of p53, which is perturbed in many human cell lines like HeLa cells.[79]

Another strong well characterized HD cell model are induced pluripotent stem cells (iPSCs). Patient derived HD fibroblasts be reprogrammed to generate iPSCs, which could then be differentiated into neurons or other cell types for cell-specific HD research.[80]

1.9 Studying huntingtin protein with fluorescence microscopy

Fluorescence microscopy is a popular way of tracking the localization and function of a protein of interest in live cells, which is usually done by tagging the protein to a fluorescent protein (FP) like GFP. However, transfecting cells with full length huntingtin fused to an FP is technically challenging; it is often toxic or not well expressed by cells.[81] In HD, many labs result to transfecting truncated exon 1 or another N-terminal fragment of huntingtin with a long polyglutamine expansion, typically longer than disease relevant lengths.[77,82] These fragments tend to overexpress, do not recapitulate whole protein, and are more prone to aggregation (even more so when fused to an FP).[83]

1.9.1 Utilizing Fluorescent Microscopy Without Fluorescent Proteins

Proteins of interest (POI) can be genetically fused to other tags that are not fluorescent but can react with substrates that add a fluorophore.[84] A popular example of this is the SNAP-tag, which requires the POI to be fused to the 20 kDa enzyme O^6-alkylguanine-DNA alkyltransferase (hAGT). The substrates are O^6-benzylguanine derivatives linked to a fluorescent dye.81 Another genetic method uses unnatural amino acid (UAA) mutagenesis to add a non-sense codon (like an amber codon) into the gene of the POI. This codon can be selectively added

to the area of interest within the protein. A second plasmid encoding aminoacyl-tRNA synthetase and tRNAs is transfected which incorporate UAA's with handles for bioorthoganol click reactions with fluorophores to the POI.[86]

Alternatively, recombinant protein can be delivered to live cells to avoid genetic transfection. The recombinant protein can be directly labelled with organic fluorophores in vitro at cysteine, lysine, or N-terminal residues.[87] Maleimide derivatives of fluorescent dyes can conjugate the dye onto the thiol group of cysteine, while amine-reactive derivatives, such as succinimidyl-esters (SE) or tetrafluorophenyl (TFP) esters conjugate the primary amines of lysine residues and the N-terminus.[88] Much variety exists in the excitation and emission spectra of these dyes, and they are smaller, can be more photostable, and brighter than fluorescent proteins.[89]

1.10 Huntingtin-lowering compounds: Current main research focus of HD therapeutics

Due to the presence of huntingtin protein aggregates found in post-mortem HD brain tissue, the toxic effects of these aggregates based on overexpression models, and aberrant protein-protein interactions exhibited by mutant huntingtin, the current therapeutic research focus in HD has been on lowering huntingtin protein.[90,91] Recent clinical trials by pharmaceutical companies Wave Life Sciences and Roche utilizes antisense oligonucleotides (ASO's) which bind to complementary strands of pre-mRNA through Watson-Crick base pairing. This binding causes either interference or degradation by RNase H, therefore reducing transcripts and protein translation.[92] These compounds were injected intrathecally as they do not cross the blood brain barrier (BBB). The ASO used by Roche was not allele selective and thus lowered both mutant and wildtype huntingtin in heterozygous HD, while Wave used an allele selective ASO to only lower mutant huntingtin.[93]

However, reducing huntingtin protein levels could raise adverse effects due to the necessity of the protein in the body and brain. For example, a reduction of wildtype huntingtin reduces vesicular transport of brain derived neurotrophic factor (BDNF) in neurons, a factor that is critical for neuronal health.[57] A counter argument that supports mutant huntingtin despite the possible consequences of wildtype lowering can be made from evidence of the age onset effect of a non-coding SNP in a nuclear factor kB (NF-κB) transcription factor binding site of the *HTT* promoter. This SNP reduces *HTT* transcriptional activity. When present on the expanded allele, the transcript lowering effect was associated with a 9.3 year delay in age onset. However, when present on the wildtype allele, the lowering of wildtype huntingtin was associated with a 3.9 year earlier age onset.[94] Some interpret this data as a net beneficial gain for HD patients because the effect of mutant huntingtin lowering seems to be more impactful than wildtype lowering based on the effect of age onset. While the Wave ASO does not affect wildtype huntingtin, this approach would not be beneficial for homozygous HD patients who do not have a copy of the wildtype gene.

Ultimately, the results from these clinical trials were unsuccessful in showing therapeutic benefit. The mutant huntingtin specific ASO from Wave was unsuccessful in phase 1b/2a trials as it did not lower huntingtin levels significantly, however the company is modifying the ASO chemistry to eventually restart clinical trials.[95] Meanwhile, the Roche ASO stopped at phase 3 as there was no beneficial effect.[96] At a recent (2021) CHDI conference, it was revealed that HD participants receiving the ASO had worse outcomes in a dose-dependent manner when compared to placebo.[95] It is uncertain if this worsening of symptoms is a direct result of wildtype huntingtin lowering, or if the ASO drug has toxic effects through another pathway.

1.10.1 Branaplam: a small molecule splicing modulator that lowers huntingtin

Other than ASO's, small molecules which alter the way huntingtin mRNA is spliced are being investigated. These compounds have the benefit that they are BBB penetrable and are delivered into the brain more effectively than ASO's.[92] One example is the compound branaplam (LMI070), which will be used in HD clinical trials this year (2021) by Novartis. Branaplam was initially discovered as a compound to treat spinal muscular atrophy (SMA) because it serves as a modulator of SMN2 (survival of motor neuron) exon 7 inclusion, which increases SMN2 production and compensates for the lack of SMN1 seen in SMA.93 During phase 1 trials of branaplam in infants with SMA, it was found branaplam had off-target effects impacting 40-50 genes, with *HTT* being one of the most significantly impacted genes. Branaplam reduces the production of *HTT* transcripts by binding to and stabilizing an intronic sequence between exons 49 and 50 which results in its inclusion in the mature transcript. This intronic sequence has a premature stop codon which results in *HTT* mRNA degradation.[98] The benefits of this drug are that it reduces huntingtin levels in a dose-dependent and reversible manner which could be safer than the ASO method.

1.11 Project Rationale

Live cell fluorescent microscopy experiments are commonly done in the Truant lab to investigate the function of huntingtin. Due to the technical challenge in transfecting full-length huntingtin, fragments of huntingtin fused to a fluorescent protein are the standard method of transfection. The fragment is usually exon 1, as it contains the disease-causing polyglutamine tract. However, this excludes most of huntingtin as full-length protein is 67 exons, which prevents effective recapitulation of disease.

To improve the current fluorescence models to study HD, we propose that transduction of fluorescently labelled recombinant huntingtin will circumvent the challenges of transfecting GFP-fusion full-length huntingtin and will be more biologically accurate than transfected GFP-fusion fragments. Since we are interested in studying the function of huntingtin in the DNA damage response and cell stress, retinal pigmented epithelial cells (RPE1) which are hTERT immortalized will be used as they have a functional p53 protein. We are able to use recombinant protein as our collaborator Dr. Rachel Harding produces huntingtin in large quantities, both in apo form or complexed with HAP40.

Moreover, Dr. Harding has shown that when HAP40 and huntingtin are translated separately for purification, they do not form complexes or interact outside of the cell. When they are co-translated, they remain in a very strong complex.[67] Utilizing this property of the recombinant protein, we can track huntingtin in response to DNA damage to learn if this function is carried out by apo-huntingtin and/or huntingtin-HAP40 complex. This method can also reveal if the cryo-EM structure of huntingtin is biologically relevant to the conformation of the protein in response to DNA damage, and if it requires HAP40 for this function.

Since Maiuri *et. al* demonstrated that huntingtin interacts with DNA damage repair enzymes upon the induction of oxidative stress, we propose to use fluorescence lifetime imaging microscopy to detect Forster resonance energy transfer (FLIM-FRET) to detect these protein-protein interactions. This would be a microscopy application of the previously described proposed method of fluorescently labelling recombinant huntingtin.

Another goal of this project involves the use of the huntingtin lowering drug branaplam, because Novartis has begun clinical trials for this drug but there is not any public data available on how branaplam affects HD. Most data for this drug is available in the context of SMA, which

is a disease affecting children immediately at birth, compared to HD which is age onset. To study the cellular effects of branaplam in HD, we will use TruHD fibroblasts. This drug will also be used to investigate if it has any downstream effects on HAP40 protein levels as a by-product of huntingtin lowering, to see if huntingtin regulates its expression levels.

Additionally, since defective DNA repair is a hallmark of HD and the huntingtin protein has some role in DNA repair, it is of interest to investigate if branaplam increases or reduces this problem. It would also be important to observe if there are any harmful consequences to lowering wildtype huntingtin in a disease where functional huntingtin is already limited due to the mutant huntingtin allele. To overcome the gap in evidence in the effectiveness of huntingtin lowering as an HD therapeutic, I propose to investigate if any changes occur to HD-associated phenotypes in a clinically relevant model like TruHD cells.

Overall, this project aims to improve current fluorescent HD models and to use the huntingtin lowering drug branaplam to investigate the relationship between huntingtin and HAP40, while also determining if branaplam can ameliorate HD phenotypes in TruHD fibroblasts.

Chapter 2: Methods and Materials

2.1 Tissue Culture

hTERT-immortalized RPE1 cells from American Type Culture Collection were grown in Dulbecco's modified Eagle's (DMEM/F12 1:1) media with 10% FBS and 0.01 mg/mL hygromycin B (Invitrogen) at 37°C with 5% CO_2. hTERT-immortalized TruHD-Q21Q18 (wildtype spousal control) and HD patient TruHD-Q43Q17 fibroblast cells[46] were cultured in minimal essential medium (MEM) with 15% FBS and 1% GlutaMax at 37°C with 5% CO_2. Unless specified, all reagents were from Life Technologies.

2.2 Branaplam (LMI070) Treatment

The powdered form of branaplam was dissolved in DMSO to make a stock concentration of 10 mM and stored at -80°C. The dissolved compound was diluted in media fresh prior to cell treatment to a concentration of 10 μM. Previous media on cells was discarded and replaced with fresh media, where the 10 μM stock of branaplam was diluted to final concentrations in the nanomolar range (ranging from 5-200 nM). For 24 hour treatments, branaplam was added to seeded plates of 70-80% confluent TruHD fibroblasts. For 72 hour treatments, branaplam was added to 50% confluent plates of TruHD fibroblasts, or 30-40% confluent RPE1 cells.

2.3 Recombinant Protein Labelling

Recombinant proteins were all provided by Dr. Rachel Harding. Proteins are produced in Sf9 cells by FLAG-tag purification, followed by high resolution size exclusion chromatography. The purified protein is concentrated in a buffer composed of 20 mM HEPES pH 7.4, 300 mM NaCl, 1 mM TCEP, 2.5% (v/v) glycerol.

Protein samples (apo-Htt and Htt-HAP40) were diluted to a concentration ranging from 1-2 mg/mL in the same buffer. A 0.2 μm nylon membrane filter centrifugal tube was equilibrated by adding sterilized protein buffer and centrifuging for 5 minutes at 10,000 x g. The flowthrough was discarded. Protein sample was then added to the equilibrated tube and centrifuged for 10 minutes at 10,000 x g in 4°C for the purpose of sterilization. The eluted protein sample was collected.

Alexa Fluor 488 TFP ester (Thermo Fisher) was diluted in a volume of 1 M $NaHCO_3$ which was $1/10^{th}$ of the volume of the protein sample. After mixing, the volume was immediately added to the protein sample to have a final concentration of 0.1 M $NaHCO_3$. This tube was wrapped in aluminum foil to prevent photobleaching and put on a rotating rack in 4°C for 6 hours. Approximately every 30 minutes, the tube was vortexed because surface tension in the small volume of the tube limited mixing.

After 6 hours, the sample was diluted by adding 3X the volume in protein buffer. A 0.5 mL 100 kDa molecular weight cut-off (MWCO) centrifugal filter (Millipore) was equilibrated by adding protein buffer and centrifuging for 5 minutes at 8,000 x g. The diluted labelled protein sample was added to the filter, and centrifuged for 2 minutes at 8,000 x g. The flowthrough was removed, then about 100 μL of protein buffer was added to the concentrated sample and pipetted well. The centrifuge step along with the addition of protein buffer was repeated twice in order to remove all unbound dye while also concentrating protein. Protein concentration was measured on a NanoVue spectrophotometer (GE Healthcare), aliquoted into tubes, flash frozen in liquid nitrogen and stored at -80°C.

2.4 Protein transduction via electroporation

RPE1 cells at 80-90% confluency were dissociated from plate using trypsin for 5 minutes. 9 mL's of DMEM:F12 1:1 media was added and cells were homogenized. 5 mL of cells were collected to be centrifuged for 500 x g for 5 minutes. After centrifugation, media was aspirated and cells were re-suspended in serum-free DMEM:F12 1:1. Centrifugation and media aspiration was repeated. Cell pellet was then resuspended in 100 µL "SF cell line" reagent (Lonza). 3-7µg of fluorescently labelled recombinant protein (either AF488-HTT or AF488-HTT-HAP40) and 2 µg of H2B-mCherry plasmid were mixed well with the cell suspension. Mixture was pipetted into electroporation cuvettes and put into the X-unit of Lonza 4D Nucleofector device. Cells were electroporated using the setting "DN-100", then removed from device and allowed to incubate at room temperature for 10-15 minutes. 500 µL of media was added to the cuvette, and this mixture was pipetted out to seed plates. 150 µL of the electroporated cell mixture was mixed with 2.25 mL of media to seed ibidi µ-Slide 8 Well chambered coverslips.

2.5 Western Blot

Cells were grown on 10 cm dishes according to section 2.1 and scraped when confluency reached 80-90%. Cells were collected in a 15 mL tube to be centrifuged at 1,500 x g for 5 minutes. The cell pellet was washed once with 1 mL of PBS, then centrifuged at 10,000 x g for 5 minutes. The cells were then lysed using radioimmunoprecipitation assay buffer (50 mM Tris-HCl pH 8.0, 150 mM NaCl, 1% NP-40, 0.25% sodium deoxycholate, 1 mM EDTA) with protease and phosphatase inhibitors (Roche) for 12 minutes on ice. Cells were then centrifuged for 12 minutes at 10,000 x g in 4°C. The supernatant was collected, and protein levels were measured by conducting a Bradford assay. 60 µg of cell lysate supernatant was denatured with

SDS loading buffer and boiled for 8 minutes, then loaded into a precast 4-20% gradient gel (Bio-Rad). The gel was then transferred to a PVDF membrane (Millipore). Membranes were blocked in TBS-T (50 mM Tris-HCl, pH 7.5, 150 mM NaCl, 0.1% Tween-20) containing 5% skim milk powder for 1 hour then cut into three sections to be probed with primary antibodies against huntingtin (Millipore MAB2166; 1:2500), HAP40 (LS-C167891, LSBio; 1:750 OR sc-69489, Santa Cruz; 1:500), and vinculin (EPR8185, Abcam; 1:2500) in the same buffer overnight at 4 °C. Membranes were washed four times with TBS-T then probed with horseradish peroxidase secondary antibodies (Abcam) for 30 minutes at room temperature. After washing as above, membranes were incubated with enhanced chemiluminescence reagent (Millipore) and imaged with a MicroChemi chemiluminescence detector (DNR Bio-imaging Systems). The Gel Analyzer function on ImageJ was used to quantify protein signal. Huntingtin and HAP40 signals were normalized to the vinculin signal from the corresponding lane.

2.6 Widefield Imaging and Measurement of Fluorescence Intensity

Quantitative immunofluorescence experiments were imaged using the EVOS FL Auto 2 inverted widefield microscope (Thermo Fisher) at 20X magnification. To avoid bias, the 405 nm light was used to find cells by nuclei, which had been stained with Hoechst. Images were also taken on locations that were spread out across the plate. CellProfiler[99] was used to analyze the images by measuring the fluorescence intensity of the specific antibody in the area encompassed by the nucleus.

2.7 Confocal Microscopy

Confocal laser scanning microscopy was used to acquire qualitative immunofluorescence images and live cell images. The Nikon A1+ confocal system was used with a PLAN APO 60/1.4 oil objective and PLAN APO 20/0.75 dry objective. Laser lines used were 405 nm, 488

nm, 561 nm, and 640 nm. Live cells were imaged in PBS with Ca^{2+} and Mg^{2+}. For overnight imaging, 10% FBS was added to this buffer.

The laser stripe assay was acquired with the Nikon C2 confocal system using a 405 nm laser with 1 ROI at 50% laser power with 1 second scanning speed.

2.8 Immunofluorescence

Cells were cultured on ibidi µ-Slide 8 Well chambered coverslips and grown to a confluency of 80-90% prior to fixation. *Methanol fixation*: Ice cold methanol was added to cells for 12 minutes and kept on a rocker in 4°C. Methanol was aspirated and cells were washed twice for 10 minutes with PBS. *Paraformaldehyde (PFA) fixation*: 4% PFA was warmed to room temperature and applied to cells for 20 minutes. Cells were washed three times for 5 minutes with PBS, then permeabilized in 0.2% Triton-X in PBS for 5 minutes. Cells were washed three times for 5 minutes with PBS. Both methods: Cells were blocked for 1 hour at room temperature in blocking buffer (10% FBS in PBS), then incubated with primary antibody diluted in blocking buffer (EPR5526, MAB2166, phospho-N17, pan-N17: diluted at 1:250. MABE1031 (PAR detection reagent) diluted at 1:500) overnight and kept on a rocker at 4°C. Cells were washed in PBS three times for 5 minutes, then a 1:500 secondary antibody solution was added at room temperature for 45 minutes. Cells were washed in PBS, then nuclei were stained with Hoechst dye 33258 (0.2 µg/mL in PBS) at room temperature for 5 minutes, then washed again. Cells were stored and imaged in PBS + 0.02% NaN_3.

2.9 FLIM-FRET Microscopy

FLIM-FRET experiments were done on the ISS Alba FastFLIM frequency domain device connected to the Nikon A1+ confocal microscope using the 60X oil objective (Nikon) using a 447 nm pulsed diode laser at a frequency of 120-200 MHz. The fluorescence signal was directed

through a 505 nm-long pass filter, and the signal emitted from the sample was split to be directed onto two photomultiplier detectors. The signal reaching the detectors was filtered through either a 475/28 nm or 520/35 nm bandpass filter (Semrock). Images were acquired at 512x512 frame size with a pixel dwell time of 12.1 μs/pixel until the photons collected reached a count of about 100, which required 20-30 frames. Image acquisition was under a minute per frame. Analysis of lifetime measurements were done using the ISS VistaVision software.

2.10 Plasmid Transfection

For the FLIM-FRET experiments, RPE1 cells were transfected with either the mCerulean-C1 plasmid (Addgene), the mCerulean-linker-YFP plasmid (cloned by Nick Caron), or the mCerulean-Htt-Q138-YFP (Nick Caron) plasmid using the chemical transfection reagent TransIT-X2 (Mirus). Cells were imaged approximately 24 hours after transfection.

2.11 Statistical Analysis

All statistical analysis and graphing were done using GraphPad Prism 9 software, except for figures 9C and 9D which used Adobe Illustrator. If only two groups were compared (as seen in Fig. 2B), a normality test was first performed. Since the data passed the normality test, a Student's t-test was done with an alpha of 0.05. For experiments that tested the effect of two independent variables on a dependent variable, an ordinary two-way ANOVA and Tukey's multiple comparisons test were performed using standard error and 95% confidence intervals. For experiments that tested if there was a correlation between two variables, linear regression was performed using 95% confidence intervals to find the coefficient of determination (R^2).

Chapter 3: Results

3.1 Optimization of ISS FLIM-FRET system for live cell use

Förster resonant energy transfer (FRET) occurs between two fluorophores. The energy from an excited donor fluorophore can be transferred to a nearby acceptor fluorophore through nonradiative dipole-dipole coupling. A donor fluorophore must be excited by a shorter (higher energy) wavelength than the acceptor, but the two must have spectral overlap.[100] An example of a donor-acceptor pair is mCerulean and YFP, which were used in the subsequent experiments. mCerulean is the donor as its peak excitation is 435 nm and its emission is 475 nm, meanwhile YFP has a peak excitation of 515 nm and emission of 530 nm.[101] Since this energy transfer can only occur if the fluorophores are under 10 nm apart, measuring FRET can be useful for detecting protein-protein interactions.[100] It is worth noting that this distance requirement is stricter and shorter in some fluorophores, such as two interacting fluorescent proteins. The shortest distance between the two for FRET is approximately under 6 nm.[102] In a biological system, the two proteins of interest (POI) in a system would be labelled by a donor or acceptor fluorophore.

In our system, FRET was detected by measuring the lifetime of the donor fluorophore (FLIM). When a fluorophore gets excited, its electrons advance to the excited state “S1”. The lifetime of the fluorophore is the amount of time it stays in this excited state before decaying and releasing a photon, which is usually measured in nanoseconds.[103] When FRET occurs between two fluorophores, the lifetime of the donor is reduced due to energy quenching. Thus, a negative FRET control of a donor alone would have a longer lifetime than a positive FRET control of a donor fluorophore interacting with an acceptor.[104]

The role of huntingtin in the DNA damage response is not well characterized. To investigate the recruitment of huntingtin to DNA in response to oxidative stress, we propose to use FLIM-FRET in RPE1 cells that are transfected with fluorescent huntingtin and histone 2B (H2B) as a DNA marker. Additionally, since DNA repair is deficient in HD cells, we propose to use FLIM-FRET to investigate interactions between DNA repair proteins such as XRCC1 and PARP1 in response to DNA damage or oxidative stress. This would be done in TruHD fibroblasts, and the DNA repair protein interaction dynamics would be compared to control fibroblasts.

The ISS FastFLIM microscope uses the frequency domain, which acquires the lifetime of fluorophores more quickly and with reduced photobleaching compared to the more commonly used time-domain FLIM system. This allows for the detection of fast and dynamic changes in protein-protein interactions.[104] Since stress and DNA damage responses in the cell are fast and inducible, this system allows us to capture changes in protein-protein interactions while also estimating the length of the interaction and the time required for these changes to occur after induced stress.

To test if the FLIM system is working, RPE1 cells were transfected with a mCerulean plasmid as a negative FRET control, which has a published lifetime of 2.9 ns.[105] The positive control was a mCerulean-linker-YFP plasmid, which encodes for two closely positioned fluorophores separated by a short linker. This control pair would be appropriate for detecting interaction between two POIs tagged to either mCerulean or YFP. These control condition cells were imaged in PBS with Ca^{2+} and Mg^{2+}, which is important to keep consistent in testing conditions because the ion composition and pH of the fluorophore's environment can impact lifetime.

The lifetime of mCerulean acquired by the device was around 2.9-3.0 ns which matches the literature. However, the lifetime of the positive control (mCerulean-linker-YFP) was the same, indicating a problem. This positive control was validated in the past by Dr Hung and Dr Caron who used it with a time-domain FLIM microscope and found a reduced lifetime of 2.3 ns. The problem was troubleshooted by first ensuring proper calibration of the microscope. This is done by imaging a dissolved dye with a known lifetime, and then adjusting the microscope settings to assign the published lifetime value to the sample. Both fluorescein dye dissolved in PBS and coumarin-6 dissolved in 100% ethanol were used for calibration. When the microscope was tested with either dye after the calibration process, the lifetime values were as expected (4.0 and 2.6, respectively).

More troubleshooting was done by adjusting the Nikon Confocal A1+ and ISS FLIM microscope settings. Eventually I found that the emission filters of the detectors on the FLIM microscope were incorrectly positioned, and a new filter was required to detect signal only arising from mCerulean, the donor fluorophore. In the positive control, I suspect that the microscope was detecting the lifetime of YFP, which was excited through FRET. An emission filter of 475 nm was used which picks up the peak emission from mCerulean but not YFP, thus only measuring the decayed lifetime of mCerulean.

Representative transfected cells with their accompanying phasor plots are seen in *Figure 2A*, which were taken from the VistaVision FLIM software. Each pixel from the image is plotted on the phasor plot, where the lifetime of a specific area in the cell can be found. For both negative and positive control cells, these pixels are centralized to a circular area on the plot, indicating that the lifetime of mCerulean is homogenous across the cell. The negative control lifetime averaged at 3.0 ns, compared to the positive control of 2.2 ns, with a standard deviation

of 0.03 and 0.08 ns respectively. This result was consistent across 3 trials, where at least 50 cells were imaged each time (Fig. 2B). Thus, it could be concluded that the microscope was correctly configured.

3.1.1 FLIM-FRET system can highlight sub-cellular areas of FRET or protein-protein interaction

The mCerulean-Htt-Q138-YFP plasmid contains exon 1 of huntingtin with a polyglutamine tract of 138. Using the time-domain FLIM system in the past, Caron and Hung transfected cells with this plasmid and saw varying levels of FRET between mCerulean and YFP depending on whether the protein was expressed diffusely or aggregated. The aggregated state of the protein caused by expanded exon 1 brings the two fluorophores close to each other, resulting in high FRET.[53]

To test the ability of the FastFLIM system to distinguish specific areas in the cell where FRET is high apart from areas where FRET is low (a heterogeneous distribution), this plasmid was transfected in RPE1 cells. The phasor plot in Figure 2C shows a more stretched-out distribution of pixels compared to the more circular area of the phasor plot in Figure 2A. By highlighting these different populations of lifetimes on the phasor plot to project onto the cell, it can be seen that areas of circular aggregates highlighted in green have a low lifetime of 2.06 ns (high FRET) compared to more diffuse areas highlighted in blue and pink where the lifetime is 2.50-2.94 ns. Thus, this proof-of-concept experiment demonstrates that the FLIM microscope can specifically highlight areas in the cell of protein-protein interactions (high FRET) apart from other areas where this interaction is not occurring.

3.2 Fluorescently labelled recombinant huntingtin can be transduced into cells

The predominant models of studying huntingtin in live cells with fluorescent microscopy uses transfected plasmid encoding htt exon 1 fused to a FP, which neglects much of (~97%) the protein. Full length huntingtin transfects poorly or is toxic to cells. To overcome these limitations, we propose fluorescently labelling full length recombinant huntingtin with a dye to then transduce it into human cells.

3.2.1 An optimized method for labelling recombinant protein with Alexa Fluor 488

Recombinant apo-Htt and Htt-HAP40 with polyglutamine lengths of 23 (Q23) were provided to us by Dr. Harding, who produces this protein in Sf9 insect cells. To fluorescently label the protein, we chose the dye Alexa Fluor 488 (AF488) TFP due to its relatively low molecular weight (643 g/mol) compared to AF dyes in the red spectra, its high photostability and brightness, and its ability to form strong carboxamide bonds.[106]

It was found that some of the protein samples had low levels of bacterial contamination which needed to be removed prior to labelling because the protein would later be transduced into live cells. This was solved by filtering protein samples through a 0.2 μm centrifugal filter prior to starting the labelling reaction.

A general antibody labelling protocol from Thermo Fisher was loosely followed with several changes made to adjust for a larger and less stable protein. The protocol suggests reacting the dye with protein for 1 hour at room temperature, but since Dr. Harding has observed degradation of huntingtin after an hour at room temperature, the reaction was done for 6 hours at 4°C instead. Because of the small protein volume, there was high surface tension in the Eppendorf reaction tube which reduced fluid movement when the tube was placed on the rotator.

To overcome this problem, the tube was removed from the rotator to be vortexed every 30 minutes.

Another factor that was tested was the pH of the reaction. A basic pH is required for conjugation of AF488 to either lysine residues or the protein N-terminus, but more residues will be labelled if the pH is increased. Although this would allow for greater signal for microscopy and therefore less protein to transfect cells, having over three AF488 labels per protein can cause artificial aggregation. Another caveat of a high pH is the increased chance for protein misfolding. Thus, the pH was adjusted to 8.1 by using a final concentration of 0.1 M $NaHCO_3$. These conditions were assessed by measuring the degree of labelling (DOL) after the protein was purified, using the equation: $DOL = \frac{A_{488} \times MW}{[protein]\varepsilon_{dye}}$ where A_{488} is the absorption of the labelled protein at 488 nm, MW is the molecular weight of the protein, and ε_{dye} is the extinction coefficient of the dye. The conditions described resulted in an average of three dye molecules per protein.

To separate the unlabelled dye from the protein, size exclusion gel filtration using Sephadex G-25 was initially attempted but resulted in loss and dilution of labelled protein. Instead, a 100 kDa MWCO concentrator centrifugal tube was used. Although this type of tube is typically used to concentrate protein samples after protein purification, it can also separate small components such as unbound dye from large proteins as it won't overload the filter. Fresh protein buffer was added to the tube until the eluate ran clear.

3.2.2 Electroporation as an effective method for protein transduction in RPE1 cells

The first attempted method of protein transduction used the chemical transduction reagent ProteoJuice (Millipore) but was very inefficient and toxic to RPE1 cells. Electroporation

was subsequently attempted because Alex et. al demonstrated proteins could be electroporated into RPE1 cells with retained functionality.[107] Since our electroporation device was not the same as this group's, electroporation settings needed to be optimized. Since we use the Lonza Nucleofector, specific settings such as voltage are not revealed to the user, and pre-set codes must be used. The DN-100 setting was successful in transducing protein and caused minimal cell death (Fig. 3). Protein and plasmid can be co-electroporated without any extra steps, which is illustrated in Figure 3 where H2B-mCherry is in red. The procedure described by Alex et. al also used centrifugation and trypsinization following electroporation to remove any non-internalized proteins which would still give off signal when imaging cells, but this was omitted because it reduced the viability and health of the RPE1 cells.

The next consideration was the quantity of protein to transduce. Too much protein would result in an overexpression system, however too little would result in low fluorescence signal. Figure 3A highlights the visual difference in transducing a low quantity of 3-5 μg or high quantity of 6-7 μg of protein with either AF488-apo-Htt or AF488-Htt-HAP40. Transducing the same micrograms of protein for both constructs result in more protein molecules for AF488-apo-Htt than AF488-Htt-HAP40 due to their differences in MW, which is why the AF488-apo-Htt images appear brighter and more concentrated with protein. Therefore, quantifying protein samples by molarity would be a more appropriate measure that should be followed in the future.

3.3 Characteristics of transduced AF488-apo-Htt and AF488-Htt-HAP40 in live RPE1 cells

3.3.1 Localization and Potential Phase Separation

By visual assessment of microscopy images, cells transfected with either AF488-apo-Htt or AF488-Htt-HAP40 have similar protein localization. Most of the protein localizes to the perinuclear space, with some diffuse localization seen in the nucleus and cytoplasm (Fig. 3). This

is consistent with the localization of endogenous full-length huntingtin, which is based off immunofluorescence.[10] Huntingtin can be found in organelles residing in the perinuclear space, such as the endoplasmic reticulum, Golgi apparatus, and mitochondria. While it cannot be confirmed that AF488-apo-Htt or AF488-Htt-HAP40 localized to these organelles as no fluorescent marker of these organelles was used, the punctate and clustered appearance of both labelled proteins resembles vesicles of the Golgi apparatus or the endoplasmic reticulum.[108,109]

Regardless of the amount of protein transfected, in a good portion of cells, both AF488-apo-Htt or AF488-Htt-HAP40 formed large 3D spherical shapes around the nuclei, with an estimated length of 3-10 μm at their longest point (white arrows in Fig. 3). It is difficult to conclude the identity of these globular shapes, as they could be protein aggregates or phase separated protein clustering with other cellular components. A Z-stack was acquired to observe the shape of these proteins from a Y-axis point of view (Fig. 3B) where the protein sphere appears to be pressing against the cell nuclei without entering. Based on time-lapse imaging of RPE1 cells, cells exhibiting these 3D protein spheres did *not* appear to die any quicker compared to cells without (data not shown). The protein spheres (white arrows) are also mobile and do not inhibit the cell's ability to divide (Fig. 4A).

3.3.2 Cells Transduced with Fluorescent Recombinant Protein Can Divide

If cells are transfected with FP-fused full length huntingtin plasmid, cells cannot divide. Our lab has also used huntingtin intrabodies fused to a FP to visualize endogenous huntingtin, however cells transfected with this plasmid also do not divide.[19] Since huntingtin has a role in mitotic orchestration[65], visualizing its localization throughout mitosis is important.

Unlike plasmid transfection, RPE1 cells transduced with either AF488-apo-Htt or AF488-Htt-HAP40 can divide. In Figure 4A, mitosis was captured by using automated imaging

overnight on the confocal microscope. Due to the spherical conformation that a cell takes during mitosis, some stages of division are not well captured (40 minute mark). Interestingly, the spherical protein cluster remained intact during and after mitosis (white arrows). In this cell and others observed, the distribution of labelled protein seems to be uneven between the two new cells.

Immunofluorescence experiments on fixed mouse neuronal cells have shown that huntingtin localizes to the spindle poles between prophase to late anaphase and to the midbody of mitotic spindles during telophase.[65] To test if labelled recombinant protein localizes appropriately during mitosis, the microtubule stain SiR-tubulin was used on RPE1 cells transduced with AF488-Htt-HAP40 16 hours prior to imaging (Fig. 4B, C, and D). In the stages of mitosis captured, the majority of AF488-Htt-HAP40 signal seems to be dispersed in punctate areas around the perimeter of the cell. During metaphase (Fig. 4B) there may be some co-localization with tubulin at the spindle poles, as pointed by the white arrows. During anaphase (Fig. 4C) a Z-stack was captured then 3D rendered on ImageJ to see if AF488-Htt-HAP40 was truly co-localizing with tubulin, or if it was hovering above or below tubulin. Although there seem to be some areas of co-localization with tubulin, AF488-Htt-HAP40 does not seem to be at the spindle poles. During telophase (Fig. 4D) the majority of AF488-Htt-HAP40 is around the perimeter of the cells, but there is a small amount found near the midbody (white arrow).

3.4 Validating signal and function of transduced AF488-apo-Htt or AF488-Htt-HAP40

3.4.1 Co-localization of recombinant protein with huntingtin antibody is variable

To ensure that the signal observed in the 488 nm channel is in fact huntingtin protein as opposed to free floating dye, immunofluorescence using four different validated huntingtin antibodies was done on transduced cells (Fig. 5). When transduced cells were fixed, the

recombinant huntingtin signal appeared to get more diffuse in some areas, but more "clumped" or "aggregated" in others compared to live cells. The distinct punctate areas of co-localization are illustrated by white arrows.

The anti-phospho-N17 antibody detects phosphorylated S13 and S16 residues and co-localizes with recombinant proteins in areas where it is diffuse and in small puncta, but poorly in areas of large "clumped" recombinant protein. The anti-N17 (pan) antibody, which detects both versions of S13 and S16, had a similar co-localization pattern with recombinant protein as anti-phospho-N17 in diffuse areas, but had more co-localization in the punctate areas. Out of all four antibodies, mAb2166 had the most overlap with areas of "clumped" or large punctate areas of protein, whereas co-localization with EPR5526 was poor.

3.4.2 Neither AF488-apo-Htt nor AF488-Htt-HAP40 reproducibly respond to oxidative stress like endogenous huntingtin

One of the desired outcomes of an improved HD fluorescence model is the ability to track the huntingtin protein in response to oxidative stress or DNA damage to learn about its role in these areas. Thus, it is imperative that labelled recombinant huntingtin retains the functionality of endogenous huntingtin. Since we are using both apo and complexed recombinant huntingtin, we expect that by testing their functionality in vivo, we can determine which conformation is required for biological functionality.

In response to oxidative stress by potassium bromate ($KBrO_3$) treatment, immunofluorescence experiments show that endogenous huntingtin localizes to the nucleus and strongly associates with chromatin like other DNA repair proteins.[19] To test if AF488-apo-Htt or AF488-Htt-HAP40 localize to the nucleus in response to $KBrO_3$, 100 mM of $KBrO_3$ (dissolved in PBS + Ca^{2+} and Mg^{2+}) was added to live cells on the microscope stage to observe if there was

a change in fluorescence intensity at the nucleus (Fig. 6). This experiment was done at least three times with each construct, however in cells transduced with AF488-apo-Htt, there was never an observed change in nuclear intensity. The nuclear fluorescence signal before and after $KBrO_3$ treatment was also quantified using CellProfiler, but no difference was observed (data not shown). In 1 out of 3 trials, AF488-Htt-HAP40 did localize to the nucleus (Fig. 6A), where fluorescence signal became more diffuse than punctate. Initially, this was interpreted as a requirement for HAP40 in the conformation of huntingtin when responding to oxidative stress. However, when this was replicated with new protein samples, the same response was not observed (Fig. 6B).

3.4.3 Neither AF488-Htt-HAP40 nor AF488-apo-Htt are recruited to stripes of DNA damage

By immunofluorescence, endogenous phospho-N17 huntingtin is recruited to stripes of DNA damage which are induced by 405 nm laser micro-irradiation.[19] This type of assay is done to study recruitment dynamics of DNA repair proteins. Therefore, we sought to replicate this experiment in live cells transduced with either AF488-Htt-HAP40 or AF488-apo-Htt as a method to test functionality of the recombinant protein, and to test if recombinant protein can be phosphorylated by endogenous kinases.

Cells transduced with either construct did not show any recruitment to the area of irradiation in the nucleus (Fig. 7). The cells were imaged for at least 10 minutes after induced damage, but there was no increase in fluorescence intensity at the stripe. This experiment was repeated twice with varying laser power levels to ensure DNA damage was induced, but the results were consistently negative.

3.4.4 AF488-Htt-HAP40 and AF488-apo-Htt have different charge/mass ratios compared to their unlabelled counterparts

Due to the unexpected negative results from the laser stripe assay and the $KBrO_3$ experiment, I questioned if the artificial modalities of the recombinant protein interfered with its biological function. For example, the AF488 conjugations made to lysine residues could interfere with post-translational modifications made to lysine, such as acylation. Additionally, the recombinant protein has a concentrated negatively charged FLAG tag, and the AF488 tags are also negatively charged. To assess the effect of AF488 tags on the recombinant protein, a native-PAGE was done with labelled and unlabelled constructs.

In Figure 8, both unlabelled protein constructs have 3-4 concentrated bands, while the corresponding labelled proteins both have one main band which is approximately at the same level as the lowest band of their unlabelled counterparts. Native-PAGE separates proteins based on charge/mass ratio, but the conformation of the protein will also influence migration. For example, the multiple bands could be caused by different protein conformations if there are denatured or unfolded forms of protein in the sample. Potential denaturing may result from protein samples being frozen at -80°C for too long. Alternatively, these multiple bands could also be due to different protein populations with varying PTMs such as glycosylation and phosphorylation, which are known to change the migration of the protein. Since htt and htt-HAP40 are large proteins (350 and 390 kDa, respectively), these bands are located at the very top of the gel. If the gel electrophoresis was conducted for a longer period of time, we may have observed more bands or better resolution of them.

The labelled protein lanes are much fainter than the unlabelled lanes, which indicates a large drop in protein quantity. Due to the difference in protein quantity across lanes, it can be

difficult to make conclusions. In both AF488-Htt-HAP40 and AF488-apo-Htt lanes, there is only one band present that is slightly higher than the 240 kDa protein ladder band. This band is at the same position for both constructs, which has migrated further than the bands in the unlabelled protein lanes. Since AF488 labels are charged and will therefore increase the net negative charge of the protein, it was expected that these samples would migrate further compared to unlabelled protein. However, these lanes have 3 fewer bands compared to their unlabelled counterparts, which suggests a loss of those protein populations

Additionally, since the AF488-Htt-HAP40 construct is 40 kDa larger than AF488-apo-Htt, it would be expected that the apo form would migrate further than the complexed form, which was not seen. If the protein was denatured during the labelling process, the HAP40 protein would be removed from the Htt-HAP40 complex and elute out of the 100 kDa MWCO filter, which could explain why the AF488-Htt-HAP40 and AF488-apo-Htt lanes are at the same position. Denatured proteins also migrate faster than folded during gel electrophoresis, which could explain why the labelled protein bands are positioned slightly lower than their unlabelled counterparts. If this is true, then it would explain the variability in protein functionality seen in sections 3.4.2 and 3.4.3. This native-PAGE was also only conducted with one batch of protein, so it should be repeated for other batches with equal quantities of proteins across lanes, and with longer gel electrophoresis times.

3.5 HAP40 protein levels are lowered as a result of huntingtin lowering

Xu et. al had shown that in *Drosophila*, depletion of HAP40 caused a reduction in huntingtin levels, suggesting a regulatory translational relationship between the two.[110] Since the results from 3.4.2 were inconclusive as to whether HAP40 is required for biologically functional huntingtin, I sought to investigate if there is a translational co-dependence of the two proteins.

Endogenous huntingtin levels were lowered in TruHDQ21Q18, TruHDQ43Q17, and RPE1 cells by treating them with the HTT splicing modulator branaplam (LMI070). This compound can lower huntingtin in a dose-dependent manner by targeting HTT pre-mRNA but does not affect HAP40 pre-mRNA. The F8A gene which codes for HAP40 also does not contain any introns, thus it cannot have alternate splicing forms.

Both treatments of 24 or 72 hours caused a reduction in huntingtin and HAP40, which was detected by Western blot (Fig. 9A and B). When quantified and normalized to the DMSO control of the cell type, in TruHD Q21Q18 cells there was a 30% decrease in huntingtin and 18% decrease in HAP40. In TruHD Q43Q17 cells, there was a 31% decrease in huntingtin and 26% decrease in HAP40 (Fig. 10C, HAP40 data not graphed). In Figure 9B, the decrease in huntingtin and HAP40 are proportional to one another as branaplam dose increases. To determine the extent of correlation between the levels of these two proteins, RPE1 cells were treated with branaplam doses lower than those used in Figure 9A to see a more gradual decrease. Western blots from three trials were quantified and normalized to the loading control (vinculin) using ImageJ (Fig. 9C). When the protein values corresponding to each dose were plotted against one another in a linear fashion, a strong correlation is seen between the two proteins with an R^2 value of 0.85 and a p-value of 6.8×10^{-8} (Fig. 9D).[111] Thus, across all three cell types used, it was found that HAP40 protein levels decrease as a result of direct huntingtin lowering.

3.6 Branaplam improves DNA damage related phenotypes in TruHD Q43Q17 cells

Phase 2 clinical trials using branaplam as a treatment for HD are commencing in 2021 with little publicly available information on the therapeutic benefit of the drug. Branaplam induces the inclusion of the intronic sequence between exons 49 and 50 which contains a stop codon, but this intronic sequence is only found in humans, and therefore the drug could only be

studied in human cells or a humanized animal. Thus, the TruHD cell lines function as a good model.

Before testing if branaplam has any effect on changing HD-associated cell phenotypes such as DNA repair, a dose response curve should be done to determine an appropriate dose for cell treatment based on the desired level of huntingtin lowering. Huntingtin protein levels were measured by western blots collected from TruHD Q43Q17 cells treated with doses of branaplam ranging from 5-200 nM for 72 hours. The western blot results from 3 trials were quantified as seen in Figure 10A and 10B. For this method of cell treatment, the estimated EC50 is around 5.596 as determined by non-linear fitting done on GraphPad. Although 72 hour treatment can reduce huntingtin levels drastically with low doses of branaplam, 24 hour treatment is also effective for moderate reduction (Fig. 10C).

In clinical trials for the Roche/IONIS HTT ASO, the goal was to reduce huntingtin levels by 50% to still allow for some huntingtin to carry out important cellular roles, while removing huntingtin that exerts toxic effects.[112] A good way to approach the question of what degree of lowering is beneficial is by testing for changes in HD phenotypes with varying doses. If there is benefit from a low dose, then this low dose should be used to avoid any potential detrimental off-target effects. Since we are interested in defective DNA damage repair as a driver of HD pathology, we tested if branaplam could ameliorate these phenotypes.

TruHD Q21Q18 and TruHD Q43Q17 cells were treated with 25 nM of branaplam for 72 hours, which lowers huntingtin by roughly 65%. At the end of the 72 hour treatment, cells were treated for 30 minutes with either PBS as a control or 100 mM $KBrO_3$ to induce DNA damage. The treatment was removed and replaced with media to allow cells to recover for 30 minutes. To examine the level of DNA damage produced, the cells were fixed to conduct

immunofluorescence against phosphorylated histone 2A (γH2AX). γH2AX is used as a quantitative marker of DNA double stranded breaks (DSB's) and can assess the extent of repair.[113] Fluorescence intensity was quantified using CellProfiler and the expected phenotype of more DNA damage was accumulated in the TruHD Q43Q17 cells compared to control TruHD Q21Q18 cells because of $KBrO_3$ treatment (Fig. 10D). However, the branaplam treated and stressed TruHD Q43Q17 cells had lower γH2AX fluorescence intensity than the untreated and stressed TruHD Q43Q17 cells (p value= 0.0324), suggesting that branaplam had an effect in reducing DSB's or increasing DNA repair.

Another HD phenotype which was found by Dr Tamara Maiuri and Carlos Barba-Bazan using the TruHD cells is elevated levels of poly ADP-ribose (PAR) in response to DNA damage or oxidative stress.[30] Elevated PAR is seen in both heterozygous HD cells (Q43Q17) and homozygous HD cells (Q50Q40). This measurement is done by treating cells with a PAR glycosylase inhibitor (PARGi) an hour before cell fixation and immunofluorescence for PAR. The fluorescence intensity of PAR is then measured using CellProfiler.[99] In the DNA damage condition, cells are treated with 100 mM of $KBrO_3$ for half an hour prior to fixation, where PARGi remains in the solution. Since PAR chains are rapidly formed by PARP and degraded by PARG, PARG must be inhibited to see the accumulation of PAR chains. When treating cells with branaplam for 24 hours at 25 nM, which lowers huntingtin by roughly 30%, PAR levels in branaplam treated and stressed TruHD Q43Q17 cells were significantly lower (p value= <0.0001) than the PAR levels of the untreated and stressed cells (Fig. 10E). Although the mean level of PAR in treated and stressed TruHD Q43Q17 cells was higher than the stressed TruHD Q21Q18 (control) cells, there was no longer a significant difference between the two. Therefore,

huntingtin lowering by branaplam by only ~30% significantly reduces the PAR levels in stressed heterozygous HD cells.

CHAPTER 4: DISCUSSION

In this project, we focused on studying the huntingtin protein and its relationship to HAP40 by optimizing fluorescent technologies for HD research and using the novel huntingtin lowering drug branaplam. Although a new FLIM-FRET system was optimized for live cell use, it has not yet been applied to study huntingtin protein-protein interactions. In chapter 5, I will discuss experiment designs for applying the optimized system to study the huntingtin protein or DNA repair dynamics in HD cells. The other fluorescent technology used was the transduction of fluorescently labelled recombinant huntingtin protein into live RPE1 cells to study the function of full-length huntingtin. If this system was validated, this protein would have been used for FLIM-FRET experiments. This chapter will discuss the findings from sections 3.2-3.6.

4.1 Potential causes for variability in transduction experiments with AF488-Htt-HAP40 or AF488-apo-Htt

Experiments in section 3.2-3.4 were done with apo or complexed constructs of recombinant protein to investigate if recombinant huntingtin exhibits the same biological functionality as endogenous huntingtin. However, the localization of huntingtin in basal conditions, during mitosis, and in response to stress or DNA damage did not always or exactly match what is expected from endogenous huntingtin. Based on the batch of protein sample used, the distribution of AF488-Htt-HAP40 or AF488-apo-Htt could range from being more diffuse and in the nucleus, to more punctate with very little nuclear localization.

In the stages of mitosis, recombinant protein did not always localize to areas endogenous huntingtin is expected to be, such as the spindle poles in anaphase (Fig. 4C). However, the ability of the transduced cells to divide demonstrated that labelled recombinant protein is not toxic to the cell, which is a problem with transfecting plasmids that encode huntingtin fused to a FP. Moreover, the referenced mitotic localization of huntingtin is based on one study where spindle pole localization was the most well-defined area.[65] Depending on the antibody used in this study, huntingtin was also found in punctate regions around the perimeter of the dividing cell, similar to Figure 4. Additionally, recombinant huntingtin might not have localized to the spindle pole as there could have already been sufficient endogenous huntingtin to carry out the necessary tasks in orchestrating mitosis.

Conversely, when testing the mobility of the protein in response to oxidative stress or DNA damage, no recombinant protein localized to the laser stripe of DNA damage, and in only one trial of $KBrO_3$ treatment did AF488-Htt-HAP40 recruit to the nucleus. Some potential explanations for this variability and negative data are as follows:

4.1.1 Potential denaturing or unfolding of protein

As seen on the native-PAGE in Figure 8, the lanes loaded with AF488 labelled proteins migrate just slightly further than the lowest band of their unlabelled counterpart. While the AF488 tag adds a negative charge to the protein, which causes further migration in native-PAGE, it is peculiar that the labelled protein does not have a slight downward shift of all 3-4 bands found in the unlabelled proteins, and instead only has one band. Additionally, the AF488-apo-Htt and AF488-Htt-HAP40 lanes have their single band in the same position, although AF488-Htt-HAP40 is 40 kDa heavier. If the protein was denatured, the HAP40 protein could have been eluted during the purification process and would explain the positioning of this band.

Denaturation or unfolding may have occurred from several factors. When the labelled protein is transduced into cell, it has been freeze-thawed for two cycles. During one of these cycles, it is out at 4°C for 6 hours. It is possible that these changes in temperature had a destabilizing effect on the protein. A way to control for this would be to redo the native-PAGE with unlabelled protein sample that has been subject to the same temperature changes as labelled protein. Alternatively, since we found that there was low levels bacterial contamination in the protein sample which increased drastically when it was transduced into cells, bacterial endotoxins could have had a detrimental effect on the protein. However, this issue was fixed by running the recombinant protein through a 0.2 μm filter to remove contaminants before labelling. If the 3-4 bands seen in the unlabelled protein lanes (Fig. 8) are unfolded protein products, then it could be due to bacteria.

Another contributor of this issue may have been the 0.2 μm centrifugal filter. This filter caused a significant loss of 50% of the starting protein sample, suggesting that a lot of protein was getting stuck on the filter. If the only protein eluting from this filter was denatured protein (which would pass through easier than folded protein because of its lack of 3D structure) then it would suggest only denatured protein is getting labelled. The filter used was made of nylon, so if this filter was switched to a low protein binding material, such as the DuraPore PVDF material, it may solve this problem.

However, these interpretations are limited due to uneven loading of protein across lanes (Fig. 8), the potential insufficient length of time that the gel electrophoresis was conducted for, and that only one batch of labelled and unlabelled protein was used as a sample source.

4.1.2 Oxidization status of protein may prevent it from responding to stress

Before huntingtin responds to oxidative stress to localize to the nucleus, the methionine 8 residue needs to be sulphoxidized.[43] This sulphoxidation also promotes S13/S16 phosphorylation, which makes huntingtin more responsive to DNA damage. Since the protein sample is kept in reducing conditions (1 mM TCEP in protein buffer) to make it more stable, it could be less prone to being oxidized and thus recruited to the nucleus. Endogenous huntingtin which could be at a higher oxidation level than recombinant may be responding to this stress because it would be more prone to S13/S16 phosphorylation than reduced recombinant protein.

4.1.3 Interference from AF488 labels

Lysine residues and the N-terminus of recombinant proteins can be conjugated to AF488, however some lysine residues have an important role in huntingtin function, so the bulky and charged AF488 groups could interfere with this. For example, lysine-6 and lysine-9 are important for huntingtin 3D conformation and are also important ubiquitination sites.[66] To circumvent this issue, a lower pH could be used in the conjugation reaction to only tag the N-terminus, or a different residue could be tagged by using a different dye, such as cysteine maleimide.

4.2 Potential phase separation of AF488-apo-Htt and AF488-Htt-HAP40

Throughout all protein transductions with either AF488-apo-Htt and AF488-Htt-HAP40, there were large round 3-dimensional areas of protein that looked like they were phase separating. Phase separation occurs in cells to enable compartmentalization without membranes, where different proteins interact with other proteins, RNA, or DNA. These compartments can undergo different phase transitions between a liquid to gel to solid state. Proteins that phase separate typically have a low complexity domain or intrinsically disordered domain (IDR).[114]

Huntingtin contains an IDR (aa's 407-665), so it is possible for it to phase separate. Furthermore, huntingtin has been found at nuclear speckles, which are phase separated subnuclear structures that contain proteins, RNA, and pre-mRNA splicing factors.[19] The presence of these structures in the cytoplasm and perinuclear space as observed in section 3.3 may suggest that huntingtin phase separation occurs outside of the nucleus as well. More experiments would need to be conducted to assess if these spherical regions are in fact phase separating, such as differential interference contrast (DIC) microscopy and fluorescence recovery after photobleaching (FRAP).

4.3 HAP40 expression is regulated by huntingtin protein levels

The huntingtin cryo-EM structure could only be solved when huntingtin was co-expressed with HAP40, but the biological relevance of this structure is unknown as not much is known about HAP40. This may be because most huntingtin protein studies are done with exon 1 fragments, and the strong interaction between huntingtin and HAP40 requires full length huntingtin.[115] Based on the strong correlation between the expression of the two proteins (Fig. 9D, $R^2 = 0.85$), evidence that targeted HAP40 lowering lowers huntingtin accordingly, and the significantly increased stability of the Htt-HAP40 complex compared to the apo-huntingtin form, we hypothesize that these two proteins are co-dependent for most likely structural purposes. If the unreproducible results from Figure 6A which demonstrated that only AF488-Htt-HAP40 responded to $KBrO_3$ stress could be reproduced by fixing the recombinant protein problems outlined in 4.1, this would suggest that the complex is required for functional reasons as well. These results also question whether huntingtin and HAP40 exist cellularly without being bound to one another. Huntingtin is known to have many protein interactors, but HAP40 has much fewer known protein interactors with the primary one being huntingtin.[10,115] Thus, it might be more likely that most, if not all, HAP40 is bound to huntingtin, but there can be relatively more

conformational forms of huntingtin existing cellularly that are bound to proteins other than HAP40.

It is not yet clear how this co-dependence is implicated in HD, but Pal et. al showed that HAP40 is elevated in HD patient derived fibroblasts.[58] I also observed this elevation in TruHD Q43Q17 fibroblasts when compared to the TruHD Q21Q18 fibroblasts and RPE1 cells (data not shown). One explanation for this could be that in human HD brains, there are elevated levels of 40-50 kDa N-terminal fragments and 30-50 kDa C-terminal fragments (partially due to caspase 3 cleavage) compared to control brains.[116,117] If the increase in huntingtin fragments could be signalling to increase HAP40 translation, HAP40 levels could increase without having full-length huntingtin to bind to, resulting in some of the cell toxicity that Pal et. al saw from HAP40 overexpression. This theory would only apply if the elevated huntingtin fragmentation and elevated HAP40 expression are found in the same cell types.

4.4 Branaplam as a Therapeutic Candidate for HD

Although there have been many clinical trials for HD therapeutics, no effective treatment has been found. However, Novartis is conducting a phase two clinical trial with the huntingtin lowering drug branaplam. Branaplam can be administered orally because it is BBB penetrable, which makes it an attractive drug candidate as it avoids the side effects caused by intrathecal injection. To determine if it has any effect on ameliorating HD cell phenotypes, I first tested its potency and efficacy for huntingtin lowering in HD heterozygous TruHD Q43Q17 fibroblasts. The drug has high potency demonstrated by its estimated EC50 for huntingtin lowering of 5.59 nM, and high efficacy demonstrated by a maximal huntingtin lowering of 86% at 200 nM (Fig 10B and C). The lowest dose of branaplam that was used to treat fibroblasts was 5 nM, so a more

accurate EC50 level can be estimated by measuring huntingtin levels in fibroblasts treated with doses lower than 5 nM.

HD fibroblasts have elevated DNA damage in response to acute oxidative stress through $KBrO_3$ treatment compared to control fibroblasts. To determine if branaplam could protect against this DNA damage, we treated fibroblasts with 25 nM branaplam for either 24 or 72 hours prior to $KBrO_3$ treatment. When treated with $KBrO_3$, γH2AX and PAR levels are significantly *higher* in HD heterozygous TruHD Q43Q17 fibroblasts compared to control TruHD Q21Q18 fibroblasts (Fig. 10D and E). This is consistent with the finding of impaired DNA repair in HD. However, when the HD cells were treated with branaplam for 24 hours (PAR) or 72 hours (γH2AX) prior to oxidative stress exposure, these levels were significantly *reduced*. Lab member Carlos Barba Bazan has also conducted comet assays to assess levels of generalized DNA damage in these two cell types in response to oxidative stress. Congruent with the PAR and γH2AX findings, he found that there was significantly less damage in the HD heterozygous cells if they had been treated with branaplam 72 hours before oxidative stress exposure. These experiments should be repeated with lower levels or shorter lengths of branaplam treatment to determine the lowest level of huntingtin lowering required to see an improvement in phenotypes.

Although we have seen positive results so far in HD heterozygous fibroblasts, it would be crucial to determine if there is any detrimental effect of huntingtin lowering on neurons. The caveat with huntingtin lowering through splicing modulators is the lack of specificity in lowering wildtype or mutant huntingtin. Wildtype huntingtin may be more disposable in fibroblasts than in neurons where it has more important functions. For example, the intrathecally injected huntingtin lowering ASO by IONIS/Roche was slightly detrimental to patients in phase 3 clinical trials. It is unknown if it was unsuccessful due to a toxic effect of the ASO unrelated to huntingtin, or if the

dose was too high and too much huntingtin was lowered. Therefore, we should proceed with caution by using the lowest dose necessary to achieve positive outcomes from removing detrimental mutant huntingtin, but not to the point of causing harm by removing too much functional wildtype huntingtin.

Chapter 5: Future Directions

5.1 Using FLIM-FRET to investigate huntingtin-DNA interaction in RPE1 cells

After finishing the optimization of the FLIM-FRET system, the original plan of this project was to use full-length AF488-Htt-HAP40 or AF488-apo-Htt co-transduced into cells with H2B-mCerulean to investigate their interaction upon DNA damage. This experimental setup would also require different controls because the fluorophores tagged to the POI's would be different than the mCerulean/YFP pair that the microscope was optimized with. An appropriate negative FRET control would be H2B-mCerulean transfected into cells alone. The positive FRET control could be recombinant H2B-mCerulean which is labelled in vitro with AF488, similar to how recombinant Htt was labelled. However, before these experiments could be done, the system of transducing cells with AF488-Htt-HAP40 or AF488-apo-Htt needs to be more thoroughly validated.

As a mitigation strategy, RPE1 cells can be transfected with a plasmid encoding huntingtin fragment 1-586 fused to YFP with H2B-mCerulean to study the interaction between huntingtin and DNA in response to oxidative stress or DNA damage. This huntingtin fragment plasmid comes in two variations of polyglutamine length (wildtype Q17 and mutant Q48), so the interaction between either wildtype or mutant huntingtin with DNA (H2B) could be compared by comparing the change in fluorescence lifetime. Since mutant huntingtin has some detrimental

effect to genomic stability by inappropriate protein-protein interactions[35], we may expect a longer or stronger interaction of mutant huntingtin with DNA compared to wildtype.

5.2 Using FLIM-FRET to investigate DNA repair protein-protein interactions in TruHD cells

DNA repair dynamics could be compared between the TruHD cell lines by doing FLIM-FRET experiments with cells transfected with plasmids encoding for DNA repair proteins XRCC1-mCerulean and PARP1-YFP. PARP1 interacts with XRCC1 when repairing DNA strand breaks, but in XRCC1 deficient cells, PARP1 becomes excessively engaged.118 In the heterozygous and homozygous HD TruHD cells, there is elevated PAR due to dysregulated PARylation dynamics. To investigate if XRCC1 has a role in this, we could measure the length and strength of interaction between XRCC1 and PARP1 after inducing DNA damage by FLIM-FRET, and compare differences in fluorescence lifetime between wildtype control cells to HD cells.

5.3 Improvements to the fluorescent recombinant protein model of studying huntingtin in live cells

Based on the inconclusive results from section 3.2-3.4 which aimed to validate the biological activity of fluorescently labelled recombinant protein (AF488-Htt-HAP40 and AF488-apo-Htt), alterations need to be made to the labelling protocol. To avoid denaturation of the protein from freeze-thaw cycles, it would be more practical to ask Dr Harding to label a batch of protein immediately after purification to avoid an extra freeze-thaw cycle. Since the Arrowsmith lab has a size exclusion chromatography (SEC) system, this method could be used to separate unlabelled dye from labelled protein instead of the 100 kDa MWCO centrifugal column. The SEC system measures the absorbance at 280 nm of the liquid fraction as it elutes and shows peaks in the fractions where protein is found. Since protein in aggregated or denatured states can

be separated based on the separate collection of protein at these peaks, the portion of the labelled properly folded protein can be separated to be used for cell transduction. To remove bacterial contaminants, nylon 0.2 um filters were used in this project, but this can be switched to DuraPore PVDF 0.2 um filters which exhibit very low protein binding and will allow for more recovery. Moreover, when the labelled protein is frozen at -80°C, it can be aliquoted with 50% glycerol to enhance stability.

To test if this new proposed purification method is more effective in retaining huntingtin conformation and structure, the microscopy experiments from section 3.2-3.4 can be repeated. An additional confirmation experiment can be done with the AF488-Htt-HAP40 and AF488-apo-Htt samples to test if there is nuclear export of recombinant protein. Since endogenous huntingtin has a nuclear export sequence, treating live cells with leptomycin B prevents this export and results in nuclear accumulation of huntingtin.[47] It would be a positive sign that the system is working if this occurs with the newly purified AF488-Htt-HAP40 and AF488-apo-Htt.

If after the proposed solutions, neither one of these new samples responded to oxidative stress as endogenous huntingtin does (as was discussed in section 3.4), the samples could be mixed with an extremely small amount of hydrogen peroxide to oxidize them before transducing the protein into cells. Alternatively, RPE1 cells could be treated with branaplam prior to transduction to lower endogenous huntingtin levels so that AF488-Htt-HAP40 or AF488-apo-Htt can replace the roles of endogenous protein.

If this system can be validated with the wildtype Q23 length recombinant huntingtin (the length used in this project), then the mutant Q54 length version of this protein that is produced by Dr. Harding should be implemented for cell transduction use as well. This would allow us to

compare any differences in protein function between the two lengths to understand more about the toxicity of mutant huntingtin.

5.4 Confirming Co-dependence of HAP40 and huntingtin by siRNA

In this project, only the dependence of HAP40 on huntingtin was shown through huntingtin lowering. However other studies in *drosophila* have shown that when HAP40 is lowered by small interfering RNA (siRNA), huntingtin is lowered accordingly.[110] Since the TruHD cells are a more clinically applicable human model, we should test if HAP40 lowering by small hairpin RNA (shRNA) or siRNA also lowers huntingtin through western blot quantification. This would determine if the relationship is co-dependent or if it is only HAP40 that is dependent on huntingtin.

5.5 Exploring other HAP40 binding partners in the absence of huntingtin

One important question this project and other recent studies on HAP40 raises is if huntingtin and HAP40 are always found bound to one another in cells, or if HAP40 is always bound to huntingtin with the existence of some promiscuous huntingtin that is bound to proteins other than HAP40. If the HAP40 shRNA/siRNA experiment suggested in 5.4 does not lower huntingtin accordingly, it would suggest the latter is more likely to be true. However, in Figure 9C, while HAP40 levels in RPE1 cells linearly decrease with huntingtin, there is slightly higher HAP40 signal compared to huntingtin which is more noticeable at the higher branaplam doses. To investigate if HAP40 has any other binding proteins in the absence of huntingtin, a co-immunoprecipitation experiment could be done on branaplam treated RPE1 cells. HAP40 could be pulled out and analyzed by mass spectrometry to identify other binding partners.

5.6 HD Phenotypes to Study with Branaplam

The HD homozygous and heterozygous TruHD fibroblasts have phenotypes distinct from control TruHD Q21Q18 fibroblasts that correlate with mouse HD models and other tissues from HD patients. Some of these include elevated DNA damage, altered cell morphology, decreased ATP/ADP ratios, and hypo-phosphorylated S13/S16 residues. In this project, we showed that branaplam has a positive effect on DNA damage repair, but these other phenotypes could be tested with branaplam treatment. Cell morphology can be assessed by conducting immunofluorescence for tubulin and staining nuclei with Hoechst and comparing the HD fibroblasts morphology to control fibroblasts through PhenoRipper analysis. The ATP/ADP ratios of treated fibroblasts can be measured with the Seahorse metabolic flux assay to determine if there is an improvement in the characteristic HD energy deficits. Finally, S13/S16 phosphorylation can be measured by quantitative immunofluorescence but should be measured relative to unphosphorylated huntingtin to determine if there is a proportional increase.

Moreover, the experiments done in this project were only conducted on HD heterozygous fibroblasts, which contain a wildtype huntingtin gene. The balance between removing enough mutant protein but keeping enough functional protein does not apply in the same way to HD homozygous individuals where both HTT genes are CAG expanded. These experiments should all be replicated in HD homozygous (Q50Q40) fibroblasts to determine if branaplam has a similar therapeutic effect, or potentially a detrimental one.

Finally, these experiments should also be conducted on HD patient derived iPSCs that have been differentiated into neurons. Since HD pathology primarily affects the brain, testing the effect of branaplam on neurons would be crucial.

5.7 Conclusion

In this project, the main goal was to create a better fluorescence model of huntingtin protein to study HD because of the saturation of research using exon1-FP fusion plasmids which primarily focuses on studying aggregation and does not recapitulate full-length huntingtin biology. While this goal was not achieved due to inconsistencies in the system and uncertainty as to whether fluorescently labelled recombinant protein functions like endogenous protein, we found that huntingtin may have phase separation properties. With the use of the huntingtin lowering drug branaplam, we also found that HAP40 is dependent on huntingtin, and there may even be a co-dependency. This instigated further research with branaplam where we optimized its dosage for use in our tissue culture model of HD, TruHD fibroblasts, to find that it has a beneficial effect on heterozygous HD cells for preventing excessive DNA damage.

Chapter 6: Figures

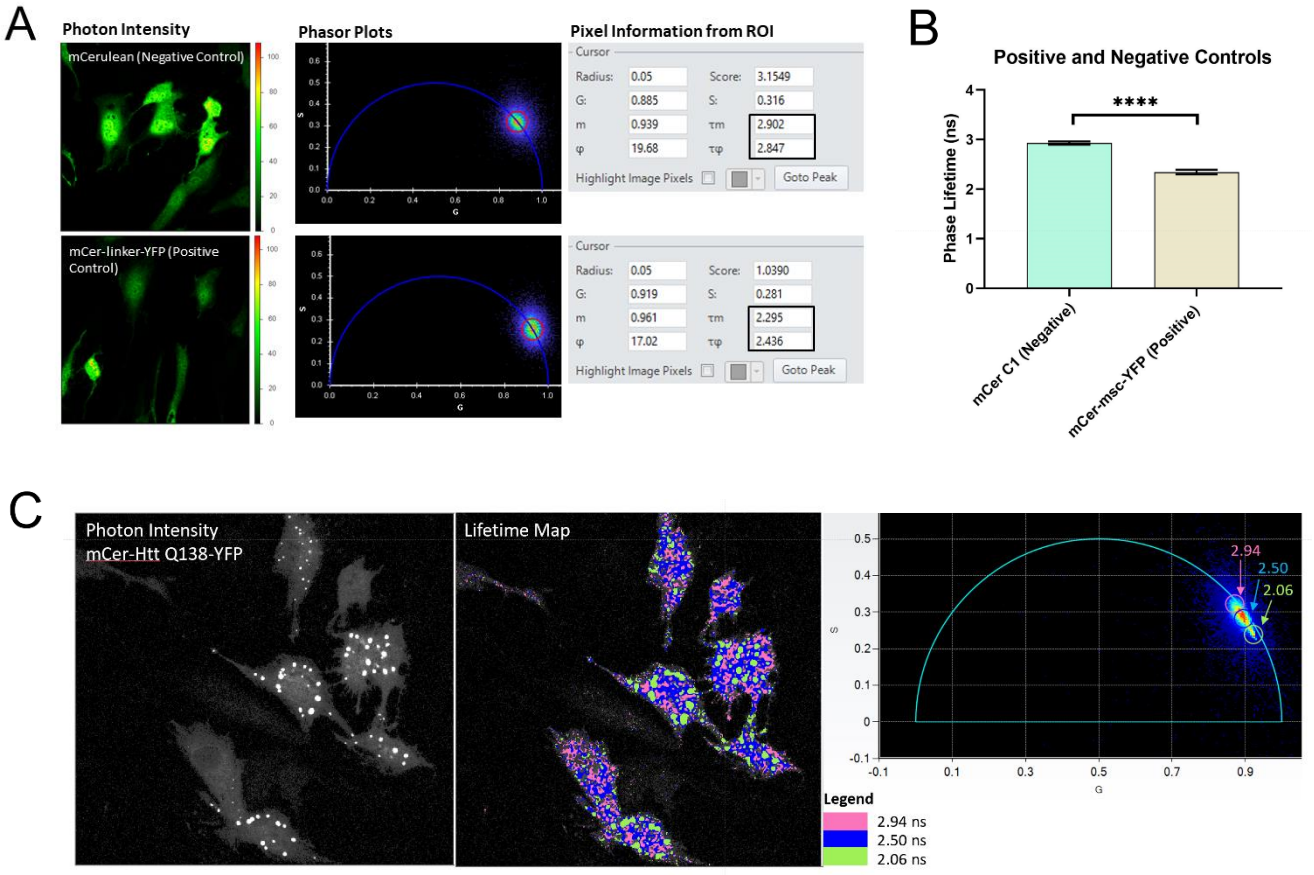

Figure 2: Lifetime acquisition using the ISS FLIM-FRET system of live RPE1 cells transfected with controls. (A) Negative FRET control mCerulean has a lifetime of about 2.9 nanoseconds, while positive FRET control mCerulean-linker-YFP has a decreased lifetime of about 2.3 nanoseconds. (B) Statistical analysis using a students t-test of lifetime measurements from transfected RPE1 cells (n=50) shows a significant difference between positive and negative controls to validate consistency in the system (N=3 trials). (C) RPE1 cells transfected with mCer-Htt Q138-YFP show three populations of lifetimes in the cell ranging from 2.06-2.94 ns. These areas are colour coded in circles on the phasor plot to show the exact location of that lifetime on the cell. Areas of circular aggregates show lower lifetime of 2.06 ns (in green) which indicates higher FRET or interaction between the two fluorophores, or the two ends of the huntingtin exon 1 fragment.

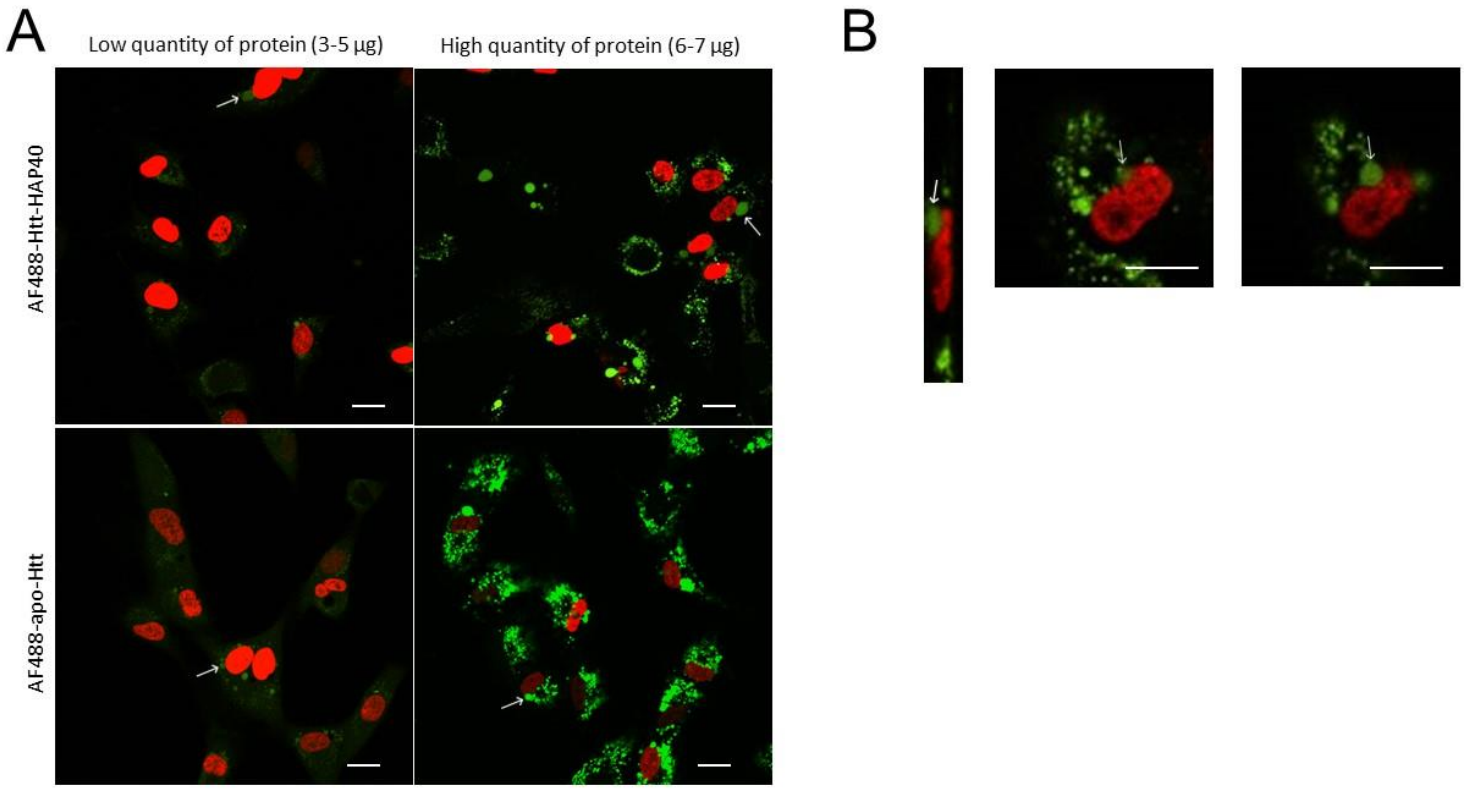

Figure 3: RPE1 cells transduced via electroporation with H2B-mCherry and either AF488-apo-Htt or AF488-Htt-HAP40. (A) Visual differences in protein depending on the amount of protein transduced. Low quantities of protein shows more diffuse localization, whereas higher quantities show more punctate forms. No visual difference is seen between AF488-apo-Htt and AF488-Htt-HAP40. When transducing either low or high protein quantity, AF488-apo-Htt and AF488-Htt-HAP40 both form potentially phase separated structures (white arrows) of varying sizes. (B) Y-axis point of view of the structure assembled on ImageJ by acquiring a Z-stack with corresponding 2-dimensional images. Scale bar represents 20 µm.

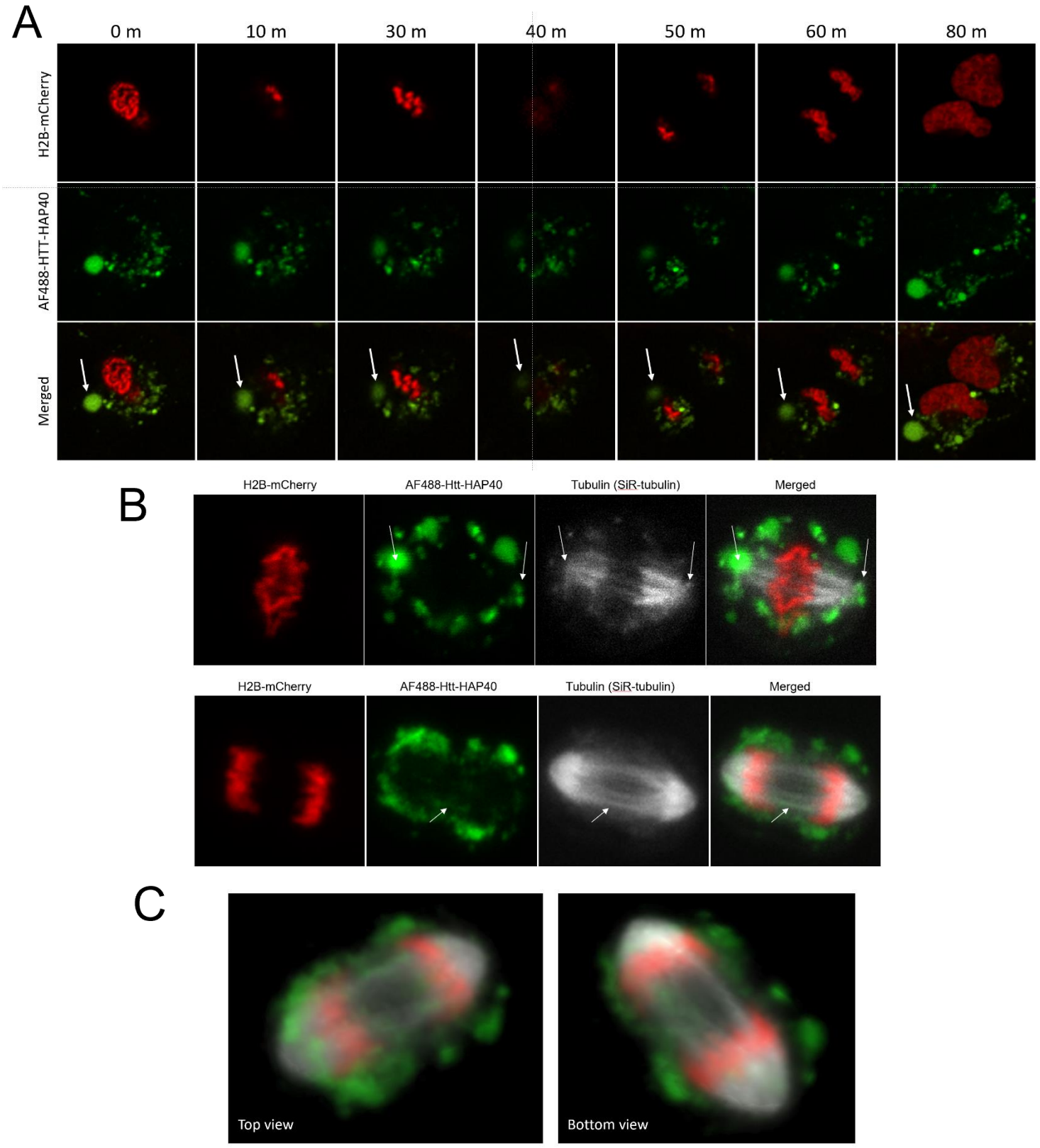
A
0 m
10 m
30 m
40 m
50 m
60 m
80 m
H2B-mCherry
AF488-HTT-HAP40
Merged
B
H2B-mCherry
AF488-Htt-HAP40
Tubulin (SiR-tubulin)
Merged
H2B-mCherry
AF488-Htt-HAP40
Tubulin (SiR-tubulin)
Merged
C
Top view
Bottom view

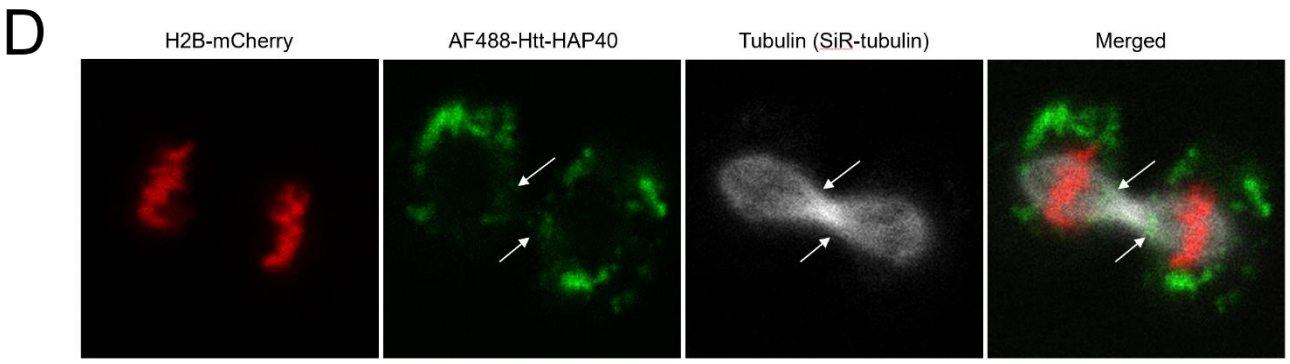

Figure 4: Localization of AF488-Htt-HAP40 in RPE1 cells in different stages of mitosis. (A) Single cell tracking shows that cells with 3D potentially phase separated or aggregated AF488-Htt-HAP40 protein (white arrow) can divide and survive after mitosis with the structure remaining intact. (B) Cell in metaphase (identified by arrangement of chromosomes) showing some co-localization between AF488-Htt-HAP40 (green) and tubulin (grey) at the spindle poles (white arrows). (C) 3D rendered images (done on ImageJ) of cell in anaphase showing little or some co-localization between AF488-Htt-HAP40 and tubulin spindle fibers. (D) Cell in telophase where the majority of AF488-Htt-HAP40 is found around the perimeter of the two newly formed cells. Some AF488-Htt-HAP40 co-localizes with tubulin at the midbody (white arrow).

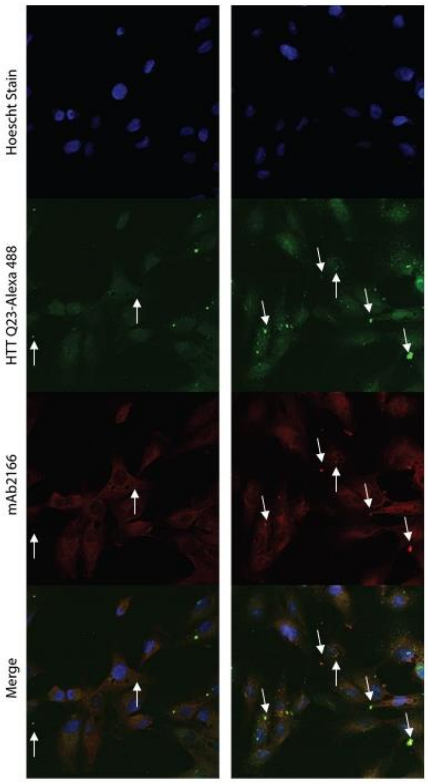
Hoescht Stain
HTT Q23-Alexa 488
mAb2166
Merge

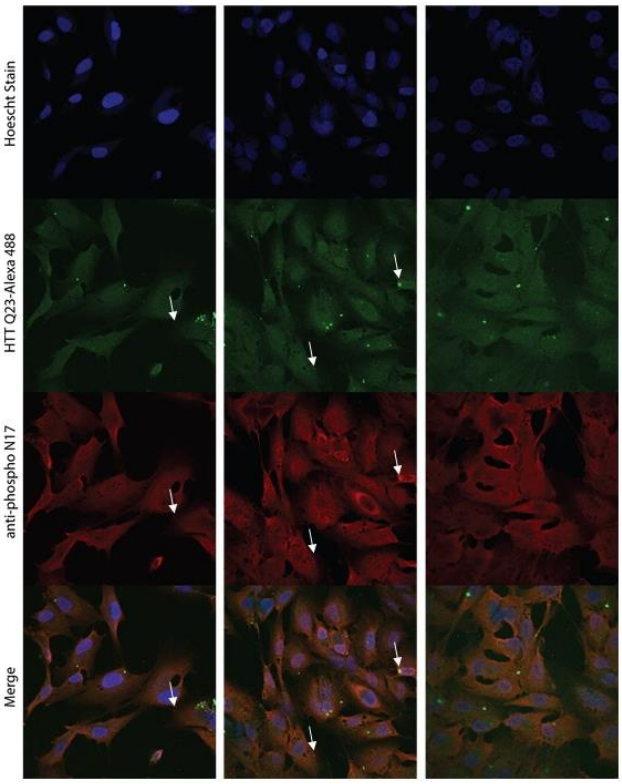
Hoescht Stain
HTT Q23-Alexa 488
anti-phospho N17
Merge

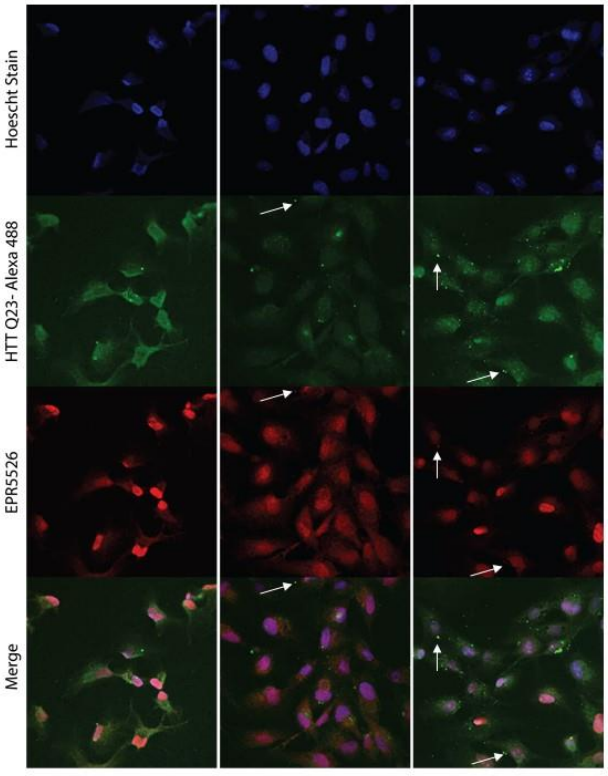
Hoescht Stain
HTT Q23- Alexa 488
EPR5526
Merge

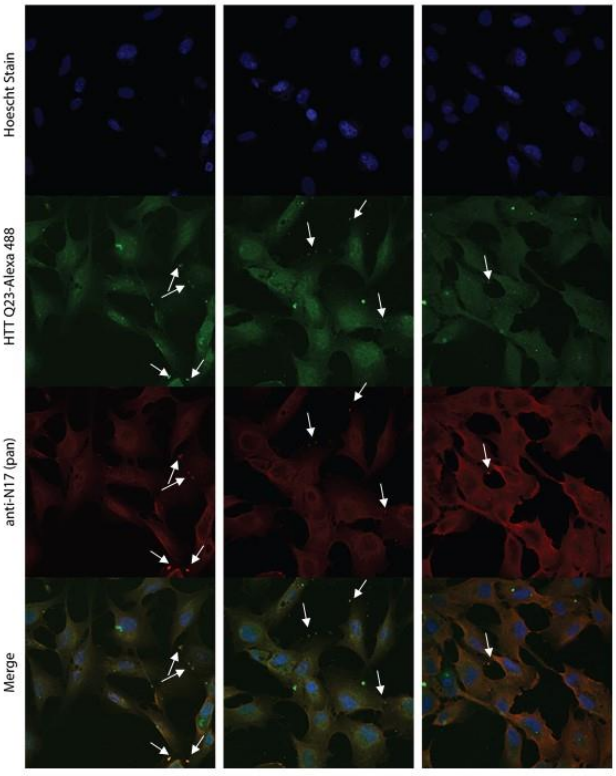
Hoescht Stain
HTT Q23-Alexa 488
anti-N17 (pan)
Merge

Figure 5: Immunofluorescence of paraformaldehyde-fixed RPE1 cells transduced with AF488-apo-Htt. Four different huntingtin antibodies were used to determine if transduced recombinant protein could be detected by antibodies. Distinct punctate areas of AF488-apo-Htt that co-localized with the antibody are shown with white arrows. Nucleus was stained with Hoechst 33342. Cells were imaged using Nikon A1 confocal at 60X magnification. Antibody used is indicated vertically along the images.

A

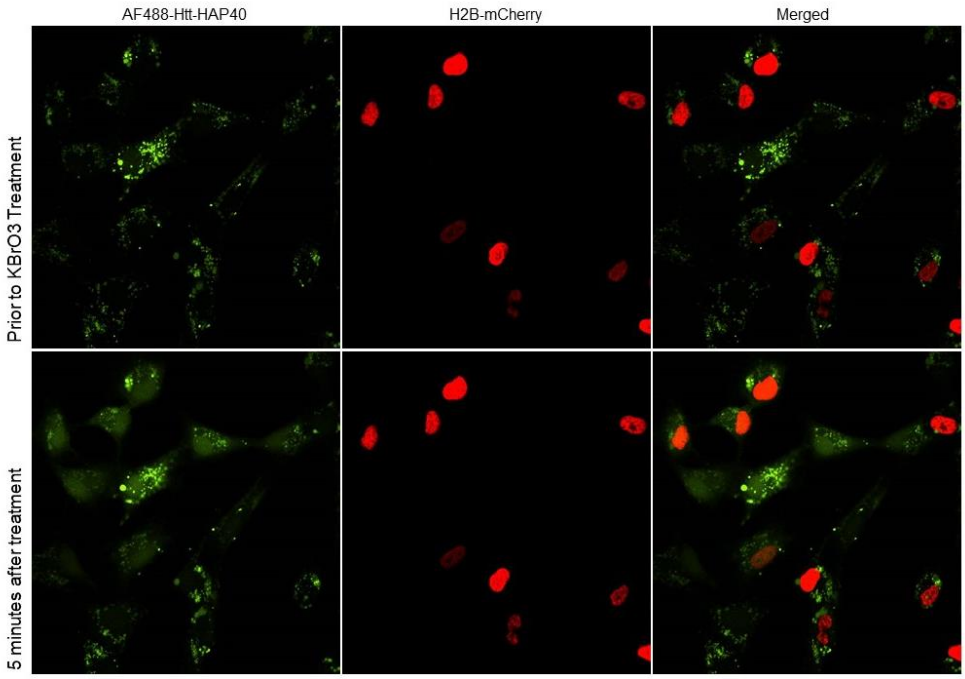
AF488-Htt-HAP40
H2B-mCherry
Merged
Prior to KBrO3 Treatment
5 minutes after treatment

B

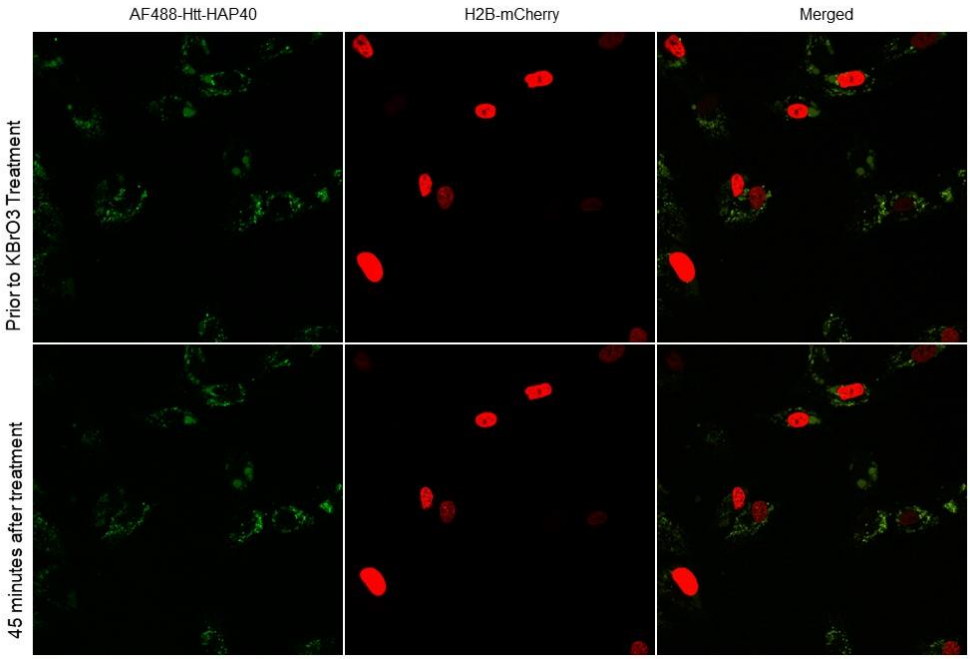
AF488-Htt-HAP40
H2B-mCherry
Merged
Prior to KBrO3 Treatment
45 minutes after treatment

Figure 6: RPE1 cells transduced with AF488-Htt-HAP40 before and after treatment with 100 mM $KBrO_3$. (A) An increase in nuclear localization of AF488-Htt-HAP40 after 5 minutes of 100 mM $KBrO_3$ treatment is seen but could not be replicated in other trials, demonstrated by (B) where there is an absence of nuclear localization. This experiment was repeated in RPE1 cells transduced with AF488-apo-Htt where there was no change in nuclear localization of huntingtin, similar to panel B.

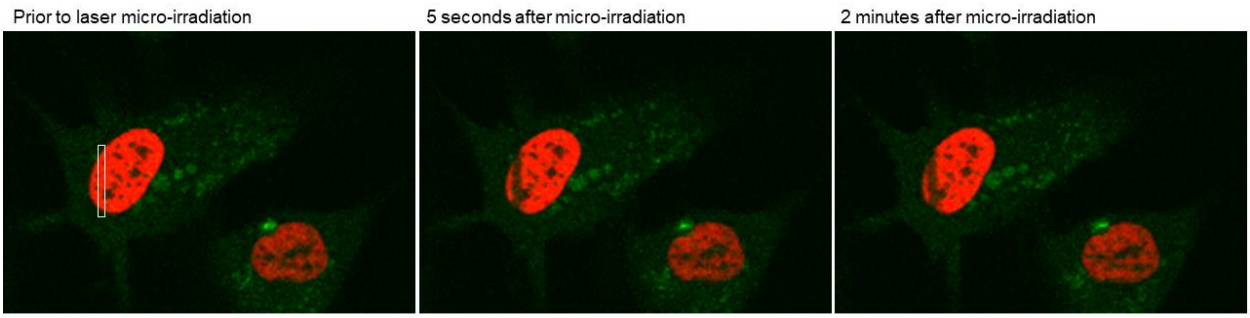

Figure 7: Laser micro-irradiation DNA damage assay conducted on RPE1 cells electroporated with AF488-apo-Htt. 405 nm wavelength laser was used to ablate the area in the white box seen in the first panel. Cells in the final panel are representative of appearance of cells 15 minutes after micro-irradiation as well. Similar results obtained for cells electroporated with AF488-Htt-HAP40. Red signal indicates H2B-mCherry, while green indicates AF488-apo-Htt. Laser micro-irradiation was done using the Nikon C2 Confocal microscope on 60X magnification.

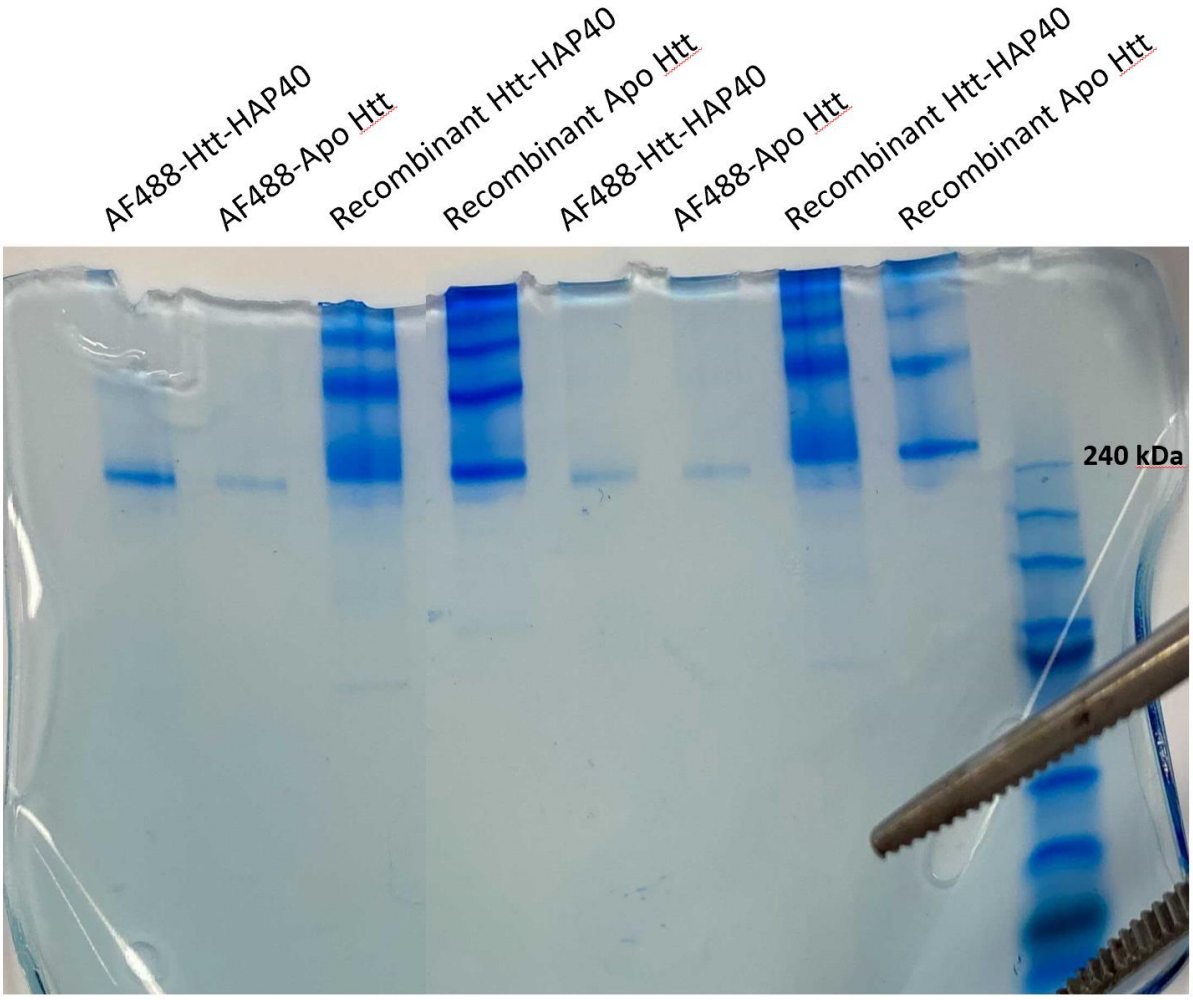

Figure 8: Native-PAGE gel loaded with labelled and unlabelled purified recombinant apo-Htt and Htt-HAP40 samples. Multiple bands are seen in the unlabelled protein lanes, which could be distinct protein populations with different post-translational modifications. In the labelled protein lanes, only one band is seen which is slightly larger than the 240 kDa marker shown by the protein ladder. Although AF488-Htt-HAP40 is 40 kDa heavier than AF488-apo-Htt, the band seen in both of these lanes migrated the same length. The loaded lanes show technical replicates of the same sample. Gel electrophoresis was done for 2.5 hours at 100 V then stained with Coomassie Brilliant Blue R-250 staining solution.

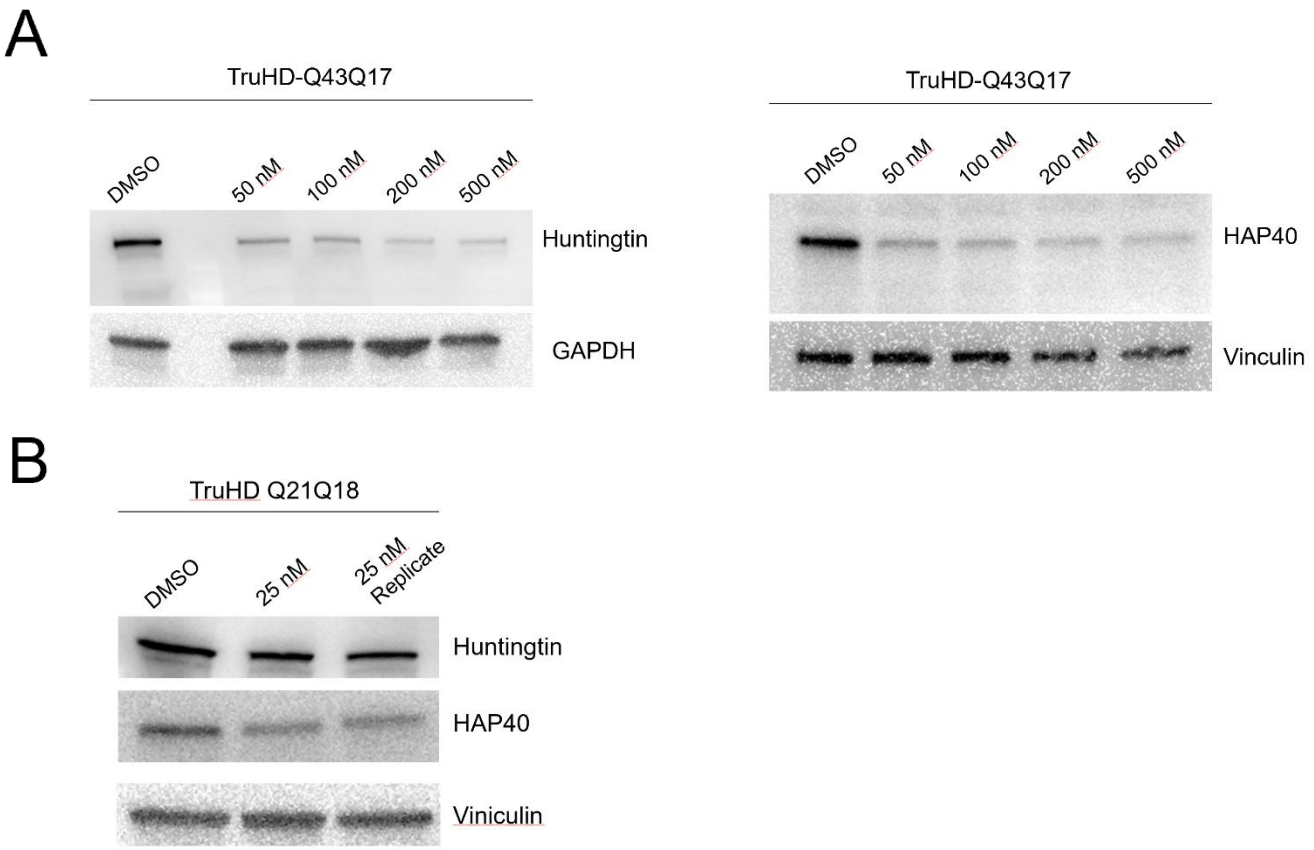
A
TruHD-Q43Q17
DMSO
50 nM
100 nM
200 nM
500 nM
Huntingtin
GAPDH
TruHD-Q43Q17
DMSO
50 nM
100 nM
200 nM
500 nM
HAP40
Vinculin
B
TruHD Q21Q18
DMSO
25 nM
25 nM Replicate
Huntingtin
HAP40
Viniculin

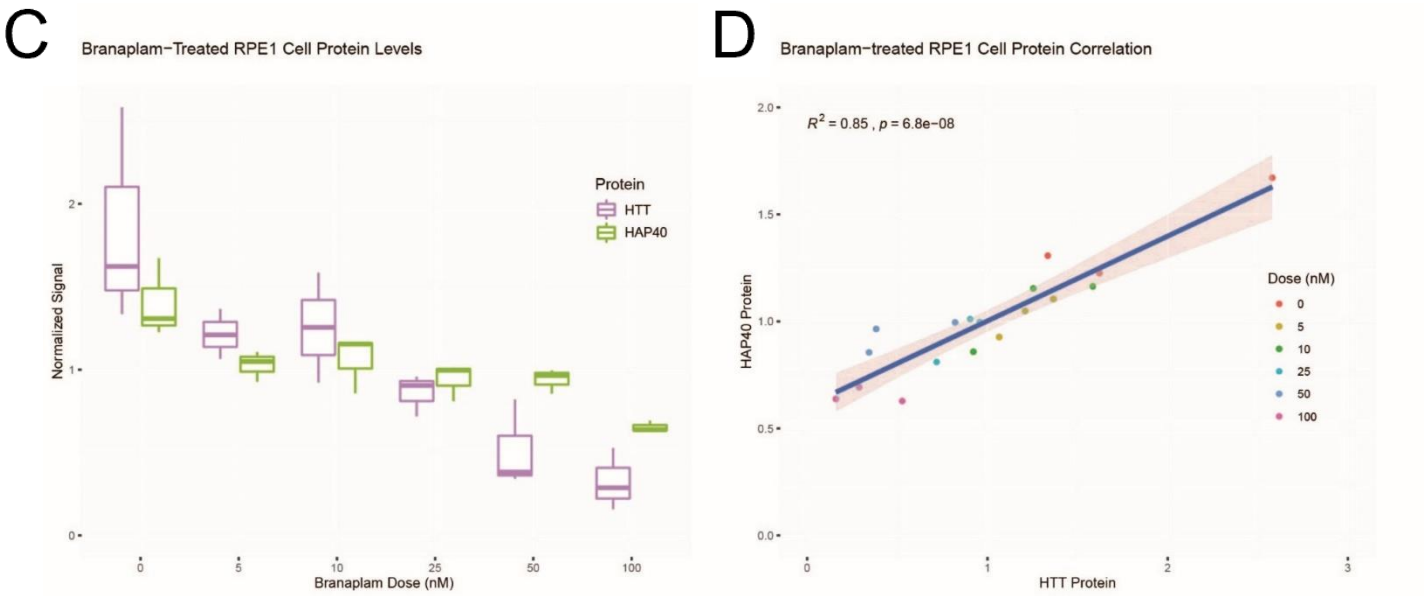
C
Branaplam−Treated RPE1 Cell Protein Levels
Protein
HTT
HAP40
Normalized Signal
Branaplam Dose (nM)
D
Branaplam−treated RPE1 Cell Protein Correlation
R^2 = 0.85 , p = 6.8e−08
HAP40 Protein
HTT Protein
Dose (nM)
0
5
10
25
50
100

Figure 9: Three different cell types demonstrate that HAP40 levels are lowered as a result of huntingtin lowering from branaplam treatment. (A) Western blot of TruHD Q43Q17 fibroblasts that were treated with varying doses of branaplam for 72 hours. Housekeeping genes GAPDH and vinculin were blotted on the same membranes as a loading control. N= 2. (B) Western blot of TruHD Q21Q18 healthy control fibroblasts that were treated with varying doses of branaplam for 24 hours at 25 nM. Vinculin was blotted on the same membrane as a loading control. N=1. (C) Quantified western blot data from 72-hour branaplam treated RPE1 cells. Western blots for HAP40 and huntingtin were quantified using Gel Analyzer on ImageJ, then values were normalized to the loading control vinculin. (D) Linear correlation (R^2 value=0.85, p-value 6.8×10^{-8}) between huntingtin and HAP40 levels corresponding to values from C. 0 nM dose of branaplam represents DMSO control. N=3

A

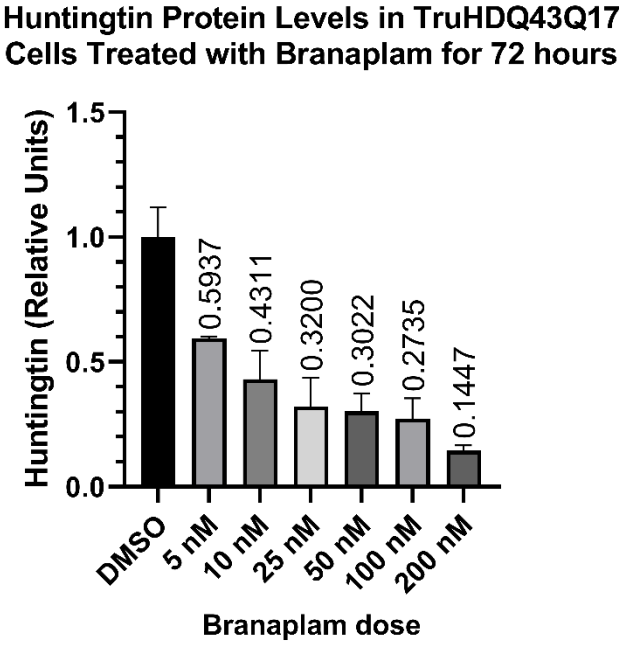
Huntingtin Protein Levels in TruHDQ43Q17
Cells Treated with Branaplam for 72 hours
Huntingtin (Relative Units)
1.5
1.0
0.5
0.0
0.5937
0.4311
0.3200
0.3022
0.2735
0.1447
DMSO
5 nM
10 nM
25 nM
50 nM
100 nM
200 nM
Branaplam dose

B

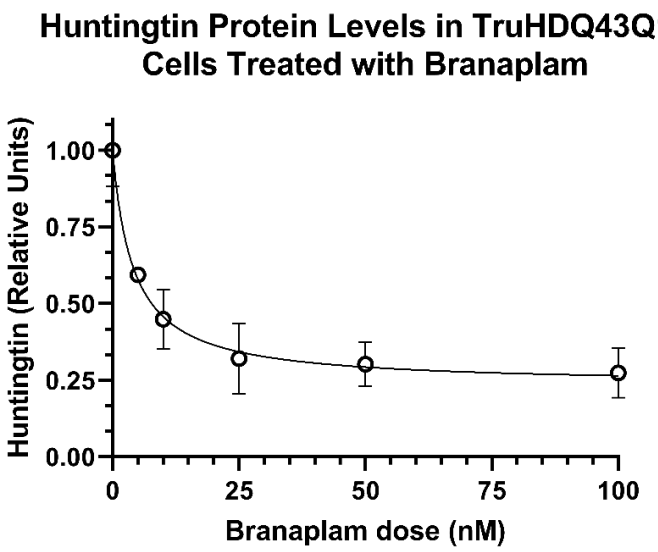
Huntingtin Protein Levels in TruHDQ43Q17
Cells Treated with Branaplam
Huntingtin (Relative Units)
1.00
0.75
0.50
0.25
0.00
0
25
50
75
100
Branaplam dose (nM)

C

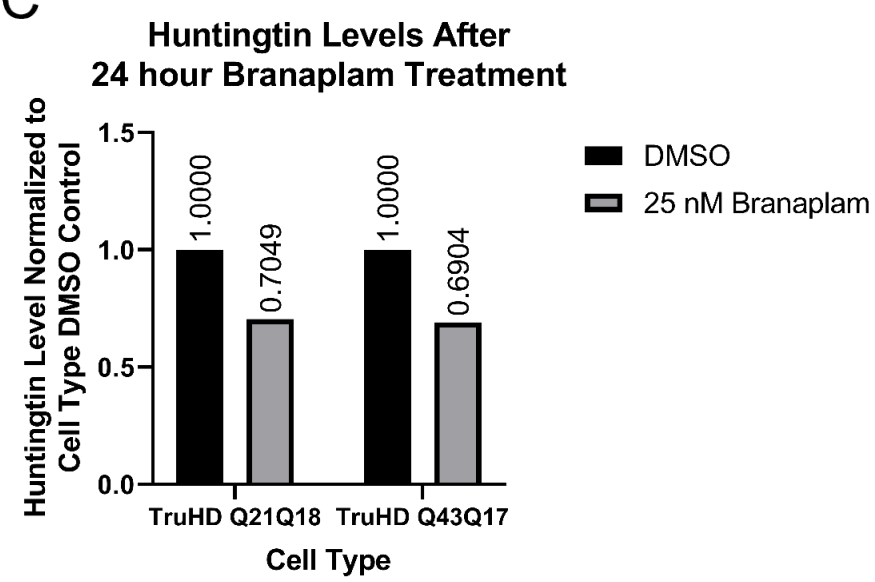
Huntingtin Levels After
24 hour Branaplam Treatment
Huntingtin Level Normalized to
Cell Type DMSO Control
1.5
1.0
0.5
0.0
1.0000
0.7049
1.0000
0.6904
TruHD Q21Q18
TruHD Q43Q17
Cell Type
DMSO
25 nM Branaplam

D

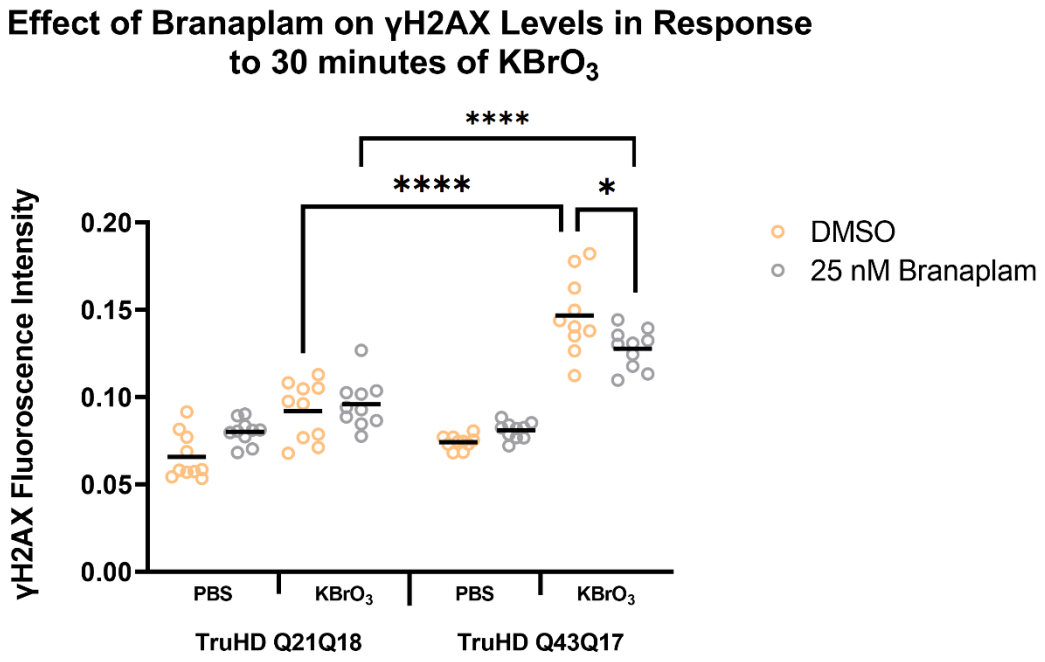
Effect of Branaplam on γH2AX Levels in Response to 30 minutes of KBrO3
γH2AX Fluorescence Intensity
0.20
0.15
0.10
0.05
0.00
****
****
*
PBS
KBrO3
PBS
KBrO3
TruHD Q21Q18
TruHD Q43Q17
DMSO
25 nM Branaplam

E

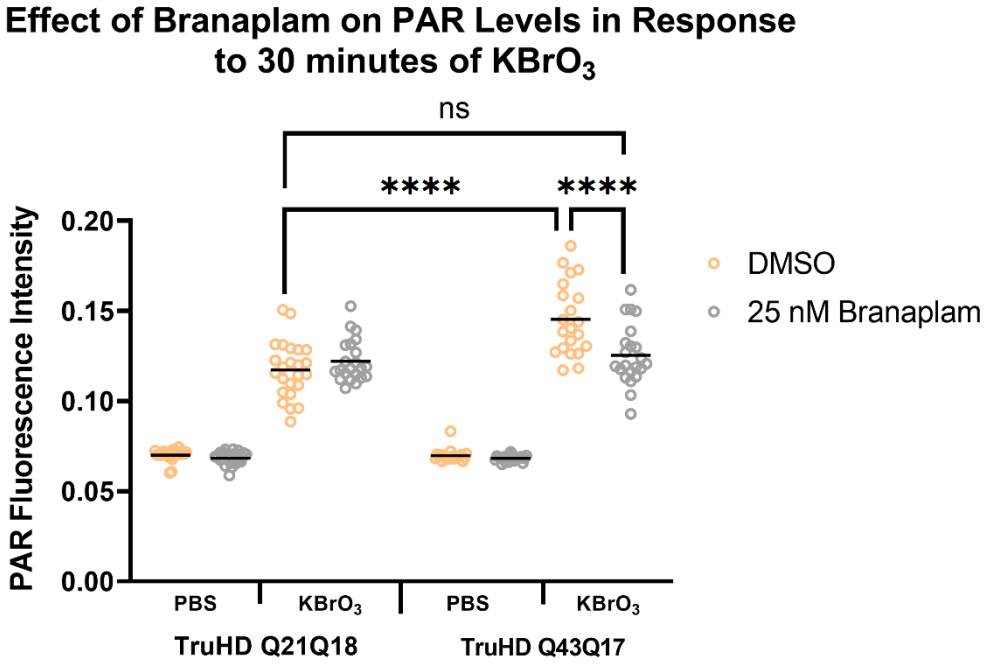
Effect of Branaplam on PAR Levels in Response to 30 minutes of KBrO3
PAR Fluorescence Intensity
0.20
0.15
0.10
0.05
0.00
ns
****
****
PBS
KBrO3
PBS
KBrO3
TruHD Q21Q18
TruHD Q43Q17
DMSO
25 nM Branaplam

Figure 10: The effect of branaplam on TruHD Q43Q17 fibroblasts. (A) and (B) Quantified western blot data from 72-hour branaplam treated Q43Q17 fibroblasts. Western blots for huntingtin (mAb2166) were quantified using Gel Analyzer on ImageJ, then values were normalized to the loading control vinculin. 200 nM value on (A) was removed for better formatting of the graph. EC50 determined from non-linear fit of 72-hour treatment was 5.59 nM. N=3 (C) Quantified western blot data from control Q21Q18 fibroblasts and HD Q43Q17 fibroblasts treated with 25 nM branaplam for 24 hours. ImageJ values were normalized to viniculin, then values were normalized again to the huntingtin value for DMSO control for each cell type. N=1 (D) γH2AX levels in control Q21Q18 and HD Q43Q17 fibroblasts in response to 30 minutes of 100 mM $KBrO_3$ treatment followed by 30 minute recovery in media to assess DNA repair response of cells. Cells were treated with 25 nM branaplam or DMSO for 72 hours prior to oxidative stress ($KBrO_3$). The branaplam treated and $KBrO_3$ stressed Q43Q17 fibroblasts had lower γH2AX fluorescence intensity than the untreated and stressed TruHD Q43Q17 fibroblasts (p value= 0.0324). N=1, n=150 cells per condition. (E) Poly ADP-ribose (PAR) levels in control Q21Q18 and HD Q43Q17 fibroblasts in response to 30 minutes of 100 mM $KBrO_3$ treatment. Cells were treated with 25 nM branaplam or DMSO for 24 hours prior to oxidative stress ($KBrO_3$). PAR levels in branaplam treated and stressed Q43Q17 fibroblasts were significantly lower (p value= <0.0001) than the PAR levels of the untreated and stressed cells, and had no statistical significance between the same condition for control Q21Q18 cells. yH2AX and PAR levels were acquired through immunofluorescence. Fluorescence intensity in the nucleus was measured by CellProfiler.

References

(1) MacDonald, M. E.; Ambrose, C. M.; Duyao, M. P.; Myers, R. H.; Lin, C.; Srinidhi, L.; Barnes, G.; Taylor, S. A.; James, M.; Groot, N.; MacFarlane, H.; Jenkins, B.; Anderson, M. A.; Wexler, N. S.; Gusella, J. F.; Bates, G. P.; Baxendale, S.; Hummerich, H.; Kirby, S.; North, M.; Youngman, S.; Mott, R.; Zehetner, G.; Sedlacek, Z.; Poustka, A.; Frischauf, A. M.; Lehrach, H.; Buckler, A. J.; Church, D.; Doucette-Stamm, L.; O'Donovan, M. C.; Riba-Ramirez, L.; Shah, M.; Stanton, V. P.; Strobel, S. A.; Draths, K. M.; Wales, J. L.; Dervan, P.; Housman, D. E.; Altherr, M.; Shiang, R.; Thompson, L.; Fielder, T.; Wasmuth, J. J.; Tagle, D.; Valdes, J.; Elmer, L.; Allard, M.; Castilla, L.; Swaroop, M.; Blanchard, K.; Collins, F. S.; Snell, R.; Holloway, T.; Gillespie, K.; Datson, N.; Shaw, D.; Harper, P. S. A Novel Gene Containing a Trinucleotide Repeat That Is Expanded and Unstable on Huntington's Disease Chromosomes. *Cell* **1993**, *72* (6), 971–983. https://doi.org/10.1016/0092-8674(93)90585-E.

(2) McColgan, P.; Tabrizi, S. J. Huntington's Disease: A Clinical Review. *European Journal of Neurology* **2018**, *25* (1), 24–34. https://doi.org/10.1111/ENE.13413.

(3) Gil, J. M.; Rego, A. C. Mechanisms of Neurodegeneration in Huntington's Disease. *European Journal of Neuroscience* **2008**, *27* (11), 2803–2820. https://doi.org/10.1111/j.1460-9568.2008.06310.x.

(4) van der Plas, E.; Langbehn, D. R.; Conrad, A. L.; Koscik, T. R.; Tereshchenko, A.; Epping, E. A.; Magnotta, V. A.; Nopoulos, P. C. Abnormal Brain Development in Child and Adolescent Carriers of Mutant Huntingtin. *Neurology* **2019**, *93* (10), E1021–E1030. https://doi.org/10.1212/WNL.0000000000008066.

(5) MacDonald, M. E.; Ambrose, C. M.; Duyao, M. P.; Myers, R. H.; Lin, C.; Srinidhi, L.; Barnes, G.; Taylor, S. A.; James, M.; Groot, N.; MacFarlane, H.; Jenkins, B.; Anderson, M. A.; Wexler, N. S.; Gusella, J. F.; Bates, G. P.; Baxendale, S.; Hummerich, H.; Kirby, S.; North, M.; Youngman, S.; Mott, R.; Zehetner, G.; Sedlacek, Z.; Poustka, A.; Frischauf, A. M.; Lehrach, H.; Buckler, A. J.; Church, D.; Doucette-Stamm, L.; O'Donovan, M. C.; Riba-Ramirez, L.; Shah, M.; Stanton, V. P.; Strobel, S. A.; Draths, K. M.; Wales, J. L.; Dervan, P.; Housman, D. E.; Altherr, M.; Shiang, R.; Thompson, L.; Fielder, T.; Wasmuth, J. J.; Tagle, D.; Valdes, J.; Elmer, L.; Allard, M.; Castilla, L.; Swaroop, M.; Blanchard, K.; Collins, F. S.; Snell, R.; Holloway, T.; Gillespie, K.; Datson, N.; Shaw, D.; Harper, P. S. A Novel Gene Containing a Trinucleotide Repeat That Is Expanded and Unstable on Huntington's Disease Chromosomes. *Cell* **1993**, *72* (6), 971–983. https://doi.org/10.1016/0092-8674(93)90585-E.

(6) Duyao, M.; Ambrose, C.; Myers, R.; Novelletto, A.; Persichetti, F.; Frontali, M.; Folstein, S.; Ross, C.; Franz, M.; Abbott, M.; Gray, J.; Conneally, P.; Young, A.; Penney, J.; Hollingsworth, Z.; Shoulson, I.; Lazzarini, A.; Falek, A.; Koroshetz, W.; Sax, D.; Bird, E.; Vonsattel, J.; Bonilla, E.; Alvir, J.; Conde, J. B.; Cha, J. H.; Dure, L.; Gomez, F.; Ramos, M.; Sanchez-Ramos, J.; Snodgrass, S.; De-Young, M.; Wexler, N.; Moscowitz, C.; Penchaszadeh, G.; Macfarlane, H.; Anderson, M.; Jenkins, B.; Srinidhi, J.; Barnes, G.; Gusella, J.; Macdonald, M. Trinucleotide Repeat Length Instability and Age of Onset in Huntington's Disease. *Nature Genetics* **1993**, *4* (4), 387–392. https://doi.org/10.1038/ng0893-387.

(7) Langbehn, D. R.; Hayden, M. R.; Paulsen, J. S.; Johnson, H.; Aylward, E.; Biglan, K.; Kieburtz, K.; Oakes, D.; Shoulson, I.; Guttman, M.; Landwehrmeyer, B. G.; Nance, M.; Ross, C.; Stout, J. CAG-Repeat Length and the Age of Onset in Huntington Disease (HD): A Review and Validation

Study of Statistical Approaches. *American Journal of Medical Genetics, Part B: Neuropsychiatric Genetics*. March 2010, pp 397–408. https://doi.org/10.1002/ajmg.b.30992.

(8) Stine, O. C.; Pleasant, N.; Franz, M. L.; Abbott, M. H.; Folstein, S. E.; Ross, C. A. Correlation between the Onset Age of Huntington's Disease and Length of the Trinucleotide Repeat in IT-15. *Human Molecular Genetics* **1993**, *2* (10), 1547–1549. https://doi.org/10.1093/hmg/2.10.1547.

(9) Paulsen, J. S.; Langbehn, D. R.; Stout, J. C.; Aylward, E.; Ross, C. A.; Nance, M.; Guttman, M.; Johnson, S.; MacDonald, M.; Beglinger, L. J.; Duff, K.; Kayson, E.; Biglan, K.; Shoulson, I.; Oakes, D.; Hayden, M.; of Iowa, U.; Carver, L. A. Detection of Huntington's Disease Decades before Diagnosis: The Predict-HD Study. **2007**. https://doi.org/10.1136/jnnp.2007.128728.

(10) Zuccato, C.; Valenza, M.; Cattaneo, E. Molecular Mechanisms and Potential Therapeutical Targets in Huntington's Disease. *Physiological Reviews*. July 2010, pp 905–981. https://doi.org/10.1152/physrev.00041.2009.

(11) Almqvist, E.; Spence, N.; Nichol, K.; Andrew, S. E.; Vesa, J.; Peltonen, L.; Anvret, M.; Goto, J.; Kanazawa, I.; Goldberg, Y. P.; Hayden, M. R. Ancestral Differences in the Distribution of the Δ2642 Glutamic Acid Polymorphism Is Associated with Varying CAG Repeat Lengths on Normal Chromosomes: Insights into the Genetic Evolution of Huntington Disease. *Human Molecular Genetics* **1995**, *4* (2), 207–214. https://doi.org/10.1093/hmg/4.2.207.

(12) Chattopadhyay, B.; Baksi, K.; Mukhopadhyay, S.; Bhattacharyya, N. P. Modulation of Age at Onset of Huntington Disease Patients by Variations in TP53 and Human Caspase Activated DNase (HCAD) Genes. *Neuroscience Letters* **2005**, *374* (2), 81–86. https://doi.org/10.1016/j.neulet.2004.10.018.

(13) Shibata, N.; Kobayashi, M. The Role for Oxidative Stress in Neurodegenerative Diseases. *Brain and Nerve*. February 2008, pp 157–170. https://doi.org/10.5607/en.2015.24.4.325.

(14) Sayre, L. M.; Perry, G.; Smith, M. A. Oxidative Stress and Neurotoxicity. **2007**. https://doi.org/10.1021/tx700210j.

(15) Lin, M. T.; Beal, M. F. Mitochondrial Dysfunction and Oxidative Stress in Neurodegenerative Diseases. *Nature*. October 19, 2006, pp 787–795. https://doi.org/10.1038/nature05292.

(16) Kregel, K. C.; Zhang, H. J. An Integrated View of Oxidative Stress in Aging: Basic Mechanisms, Functional Effects, and Pathological Considerations. *https://doi.org/10.1152/ajpregu.00327.2006* **2007**, *292* (1), 18–36. https://doi.org/10.1152/AJPREGU.00327.2006.

(17) Ayala-Peña, S. Role of Oxidative DNA Damage in Mitochondrial Dysfunction and Huntington's Disease Pathogenesis. *Free Radical Biology and Medicine*. Elsevier Inc. 2013, pp 102–110. https://doi.org/10.1016/j.freeradbiomed.2013.04.017.

(18) JD, L.; WR, M.; AR, J.; BR, L.; JS, P. 8OHdG as a Marker for Huntington Disease Progression. *Neurobiology of disease* **2012**, *46* (3), 625–634. https://doi.org/10.1016/J.NBD.2012.02.012.

(19) Maiuri, T.; Mocle, A. J.; Hung, C. L.; Xia, J.; van Roon-Mom, W. M. C.; Truant, R. Huntingtin Is a Scaffolding Protein in the ATM Oxidative DNA Damage Response Complex. *Human Molecular Genetics* **2016**, ddw395. https://doi.org/10.1093/hmg/ddw395.

(20) Browne, S. E.; Bowling, A. C.; MacGarvey, U.; Baik, M. J.; Berger, S. C.; Muqit, M. M. K.; Bird, E. D.; Beal, M. F. Oxidative Damage and Metabolic Dysfunction in Huntington's Disease: Selective Vulnerability of the Basal Ganglia. *Annals of Neurology* **1997**, *41* (5), 646–653. https://doi.org/10.1002/ana.410410514.

(21) Askeland, G.; Dosoudilova, Z.; Rodinova, M.; Klempir, J.; Liskova, I.; Kuśnierczyk, A.; Bjørås, M.; Nesse, G.; Klungland, A.; Hansikova, H.; Eide, L. Increased Nuclear DNA Damage Precedes Mitochondrial Dysfunction in Peripheral Blood Mononuclear Cells from Huntington's Disease Patients. *Scientific Reports* **2018**, *8* (1). https://doi.org/10.1038/s41598-018-27985-y.

(22) Lin, Y.; Dent, S. Y. R.; Wilson, J. H.; Wells, R. D.; Napierala, M. R Loops Stimulate Genetic Instability of CTG·CAG Repeats. *Proceedings of the National Academy of Sciences of the United States of America* **2010**, *107* (2), 692–697. https://doi.org/10.1073/pnas.0909740107.

(23) Mangiarini, L.; Sathasivam, K.; Mahal, A.; Mott, R.; Seller, M.; Bates, G. P. Instability of Highly Expanded CAG Repeats in Mice Transgenic for the Huntington's Disease Mutation. *Nature Genetics* **1997**, *15* (2), 197–200. https://doi.org/10.1038/ng0297-197.

(24) Castel, A. L.; Cleary, J. D.; Pearson, C. E. Repeat Instability as the Basis for Human Diseases and as a Potential Target for Therapy. *Nature Reviews Molecular Cell Biology*. March 2010, pp 165–170. https://doi.org/10.1038/nrm2854.

(25) Swami, M.; Hendricks, A. E.; Gillis, T.; Massood, T.; Mysore, J.; Myers, R. H.; Wheeler, V. C. Somatic Expansion of the Huntington's Disease CAG Repeat in the Brain Is Associated with an Earlier Age of Disease Onset. *Human Molecular Genetics* **2009**, *18* (16), 3039–3047. https://doi.org/10.1093/hmg/ddp242.

(26) Aronin, N.; Chase, K.; Young, C.; Sapp, E.; Schwarz, C.; Matta, N.; Kornreich, R.; Lanwehrmeyer, B.; Bird, E.; Beal, M. F.; Vonsattel, J. P.; Smith, T.; Carraway, R.; Boyce, F. M.; Young, A. B.; Penney, J. B.; DiFiglia, M. CAG Expansion Affects the Expression of Mutant Huntingtin in the Huntington's Disease Brain. *Neuron* **1995**, *15* (5), 1193–1201. https://doi.org/10.1016/0896-6273(95)90106-X.

(27) Lee, J. M.; Wheeler, V. C.; Chao, M. J.; Vonsattel, J. P. G.; Pinto, R. M.; Lucente, D.; Abu-Elneel, K.; Ramos, E. M.; Mysore, J. S.; Gillis, T.; MacDonald, M. E.; Gusella, J. F.; Harold, D.; Stone, T. C.; Escott-Price, V.; Han, J.; Vedernikov, A.; Holmans, P.; Jones, L.; Kwak, S.; Mahmoudi, M.; Orth, M.; Landwehrmeyer, G. B.; Paulsen, J. S.; Dorsey, E. R.; Shoulson, I.; Myers, R. H. Identification of Genetic Factors That Modify Clinical Onset of Huntington's Disease. *Cell* **2015**, *162* (3), 516–526. https://doi.org/10.1016/j.cell.2015.07.003.

(28) Cardinale, A.; Paldino, E.; Giampà, C.; Bernardi, G.; Fusco, F. R. PARP-1 Inhibition Is Neuroprotective in the R6/2 Mouse Model of Huntington's Disease. *PLOS ONE* **2015**, *10* (8), e0134482. https://doi.org/10.1371/journal.pone.0134482.

(29) Ray Chaudhuri, A.; Nussenzweig, A. The Multifaceted Roles of PARP1 in DNA Repair and Chromatin Remodelling. *Nature Publishing Group* **2017**, *18*. https://doi.org/10.1038/nrm.2017.53.

(30) Maiuri, T.; Truant, R. ROS-Specific Huntingtin Interactions: Testing PARG Activity in HD Patient Fibroblasts. **2019**. https://doi.org/10.5281/ZENODO.3560227.

(31) Holton, N. W.; Andrews, J. F.; Gassman, N. R. Application of Laser Micro-Irradiation for Examination of Single and Double Strand Break Repair in Mammalian Cells. *Journal of Visualized Experiments : JoVE* **2017**, *2017* (127), 56265. https://doi.org/10.3791/56265.

(32) Smith, J.; Mun Tho, L.; Xu, N.; A. Gillespie, D. The ATM–Chk2 and ATR–Chk1 Pathways in DNA Damage Signaling and Cancer. *Advances in Cancer Research* **2010**, *108* (C), 73–112. https://doi.org/10.1016/B978-0-12-380888-2.00003-0.

(33) CJ, B.; MB, K. DNA Damage Activates ATM through Intermolecular Autophosphorylation and Dimer Dissociation. *Nature* **2003**, *421* (6922), 499–506. https://doi.org/10.1038/NATURE01368.

(34) Lu, X. H.; Mattis, V. B.; Wang, N.; Al-Ramahi, I.; van den Berg, N.; Fratantoni, S. A.; Waldvogel, H.; Greiner, E.; Osmand, A.; Elzein, K.; Xiao, J.; Dijkstra, S.; de Pril, R.; Vinters, H. v.; Faull, R.; Signer, E.; Kwak, S.; Marugan, J. J.; Botas, J.; Fischer, D. F.; Svendsen, C. N.; Munoz-Sanjuan, I.; Yang, X. W. Targeting ATM Ameliorates Mutant Huntingtin Toxicity in Cell and Animal Models of Huntington's Disease. *Science Translational Medicine* **2014**, *6* (268), 268ra178. https://doi.org/10.1126/scitranslmed.3010523.

(35) Enokido, Y.; Tamura, T.; Ito, H.; Arumughan, A.; Komuro, A.; Shiwaku, H.; Sone, M.; Foulle, R.; Sawada, H.; Ishiguro, H.; Ono, T.; Murata, M.; Kanazawa, I.; Tomilin, N.; Tagawa, K.; Wanker, E. E.; Okazawa, H. Mutant Huntingtin Impairs Ku70-Mediated DNA Repair. *Journal of Cell Biology* **2010**, *189* (3), 425–443. https://doi.org/10.1083/jcb.200905138.

(36) Gao, R.; Chakraborty, A.; Geater, C.; Pradhan, S.; Gordon, K. L.; Snowden, J.; Yuan, S.; Dickey, A. S.; Choudhary, S.; Ashizawa, T.; Ellerby, L. M.; la Spada, A. R.; Thompson, L. M.; Hazra, T. K.; Sarkar, P. S. Mutant Huntingtin Impairs PNKP and ATXN3, Disrupting DNA Repair and Transcription. *eLife* **2019**, *8*. https://doi.org/10.7554/ELIFE.42988.

(37) Li, S. H.; Schilling, G.; Young, W. S.; Li, X.; Margolis, R. L.; Stine, O. C.; Wagster, M. v.; Abbott, M. H.; Franz, M. L.; Ranen, N. G.; Folstein, S. E.; Hedreen, J. C.; Ross, C. A. Huntington's Disease Gene (IT15) Is Widely Expressed in Human and Rat Tissues. *Neuron* **1993**, *11* (5), 985–993. https://doi.org/10.1016/0896-6273(93)90127-D.

(38) Guo, Q.; Huang, B.; Cheng, J.; Seefelder, M.; Engler, T.; Pfeifer, G.; Oeckl, P.; Otto, M.; Moser, F.; Maurer, M.; Pautsch, A.; Baumeister, W.; Fernández-Busnadiego, R.; Kochanek, S. The Cryo-Electron Microscopy Structure of Huntingtin. *Nature* **2018**, *555* (7694), 117–120. https://doi.org/10.1038/nature25502.

(39) Saudou, F.; Humbert, S. The Biology of Huntingtin. *Neuron* **2016**, *89* (5), 910–926. https://doi.org/10.1016/J.NEURON.2016.02.003.

(40) Tartari, M.; Gissi, C.; lo Sardo, V.; Zuccato, C.; Picardi, E.; Pesole, G.; Cattaneo, E. Phylogenetic Comparison of Huntingtin Homologues Reveals the Appearance of a Primitive PolyQ in Sea Urchin. *Molecular Biology and Evolution* **2008**, *25* (2), 330–338. https://doi.org/10.1093/molbev/msm258.

(41) Ho, L. W.; Carmichael, J.; Swartz, J.; Wyttenbach, A.; Rankin, J.; Rubinsztein, D. C. The Molecular Biology of Huntington's Disease. *Psychological Medicine*. 2001, pp 3–14. https://doi.org/10.1017/S0033291799002871.

(42) Cattaneo, E.; Zuccato, C.; Tartari, M. Normal Huntingtin Function: An Alternative Approach to Huntington's Disease. *Nature Reviews Neuroscience*. December 2005, pp 919–930. https://doi.org/10.1038/nrn1806.

(43) DiGiovanni, L. F.; Mocle, A. J.; Xia, J.; Truant, R. Huntingtin N17 Domain Is a Reactive Oxygen Species Sensor Regulating Huntingtin Phosphorylation and Localization. *Human Molecular Genetics* **2016**, *25* (18), 3937–3945. https://doi.org/10.1093/hmg/ddw234.

(44) Atwal, R. S.; Desmond, C. R.; Caron, N.; Maiuri, T.; Xia, J.; Sipione, S.; Truant, R. Kinase Inhibitors Modulate Huntingtin Cell Localization and Toxicity. *Nature Chemical Biology* **2011**, *7* (7), 453–460. https://doi.org/10.1038/nchembio.582.

(45) Bowie, L. E.; Maiuri, T.; Alpaugh, M.; Gabriel, M.; Arbez, N.; Galleguillos, D.; Hung, C. L. K.; Patel, S.; Xia, J.; Hertz, N. T.; Ross, C. A.; Litchfield, D. W.; Sipione, S.; Truant, R. N6-Furfuryladenine Is Protective in Huntington's Disease Models by Signaling Huntingtin Phosphorylation. *Proceedings of the National Academy of Sciences of the United States of America* **2018**, *115* (30), E7081–E7090. https://doi.org/10.1073/pnas.1801772115.

(46) Hung, C. L. K.; Maiuri, T.; Bowie, L. E.; Gotesman, R.; Son, S.; Falcone, M.; Giordano, J. V.; Gillis, T.; Mattis, V.; Lau, T.; Kwan, V.; Wheeler, V.; Schertzer, J.; Singh, K.; Truant, R. A Patient-Derived Cellular Model for Huntington's Disease Reveals Phenotypes at Clinically Relevant CAG Lengths. *Molecular Biology of the Cell* **2018**, *29* (23), 2809–2820. https://doi.org/10.1091/mbc.E18-09-0590.

(47) Xia, J.; Lee, D. H.; Taylor, J.; Vandelft, M.; Truant, R. Huntingtin Contains a Highly Conserved Nuclear Export Signal. *Human Molecular Genetics* **2003**, *12* (12), 1393–1403. https://doi.org/10.1093/hmg/ddg156.

(48) Ross, C. A.; Poirier, M. A. Protein Aggregation and Neurodegenerative Disease. *Nature Medicine* **2004**, *10* (7), S10. https://doi.org/10.1038/nm1066.

(49) Eisele, Y. S.; Monteiro, C.; Fearns, C.; Encalada, S. E.; Wiseman, R. L.; Powers, E. T.; Kelly, J. W. Targeting Protein Aggregation for the Treatment of Degenerative Diseases. *Nature reviews. Drug discovery* **2015**, *14* (11), 759. https://doi.org/10.1038/NRD4593.

(50) Doody, R. S.; Raman, R.; Farlow, M.; Iwatsubo, T.; Vellas, B.; Joffe, S.; Kieburtz, K.; He, F.; Sun, X.; Thomas, R. G.; Aisen, P. S.; Siemers, E.; Sethuraman, G.; Mohs, R. A Phase 3 Trial of Semagacestat for Treatment of Alzheimer's Disease. *http://dx.doi.org/10.1056/NEJMoa1210951* **2013**, *369* (4), 341–350. https://doi.org/10.1056/NEJMOA1210951.

(51) DiFiglia, M.; Sapp, E.; Chase, K. O.; Davies, S. W.; Bates, G. P.; Vonsattel, J. P.; Aronin, N. Aggregation of Huntingtin in Neuronal Intranuclear Inclusions and Dystrophic Neurites in Brain. *Science* **1997**, *277* (5334), 1990–1993. https://doi.org/10.1126/SCIENCE.277.5334.1990.

(52) Arrasate, M.; Mitra, S.; Schweitzer, E. S.; Segal, M. R.; Finkbeiner, S. Inclusion Body Formation Reduces Levels of Mutant Huntingtin and the Risk of Neuronal Death. *Nature*. October 14, 2004, pp 805–810. https://doi.org/10.1038/nature02998.

(53) Caron, N. S.; Hung, C. L.; Atwal, R. S.; Truant, R. Live Cell Imaging and Biophotonic Methods Reveal Two Types of Mutant Huntingtin Inclusions. *Human Molecular Genetics* **2014**, *23* (9), 2324–2338. https://doi.org/10.1093/HMG/DDT625.

(54) Illuzzi, J.; Yerkes, S.; Parekh-Olmedo, H.; Kmiec, E. B. DNA Breakage and Induction of DNA Damage Response Proteins Precede the Appearance of Visible Mutant Huntingtin Aggregates. *Journal of Neuroscience Research* **2009**, *87* (3), 733–747. https://doi.org/10.1002/jnr.21881.

(55) Nasir, J.; Floresco, S. B.; O'Kusky, J. R.; Diewert, V. M.; Richman, J. M.; Zeisler, J.; Borowski, A.; Marth, J. D.; Phillips, A. G.; Hayden, M. R. Targeted Disruption of the Huntington's Disease Gene Results in Embryonic Lethality and Behavioral and Morphological Changes in Heterozygotes. *Cell* **1995**, *81* (5), 811–823. https://doi.org/10.1016/0092-8674(95)90542-1.

(56) Hodgson, J. G.; Smith, D. J.; McCutcheon, K.; Koide, H. B.; Nishiyama, K.; Dinulos, M. B.; Stevens, M. E.; Bissada, N.; Nasir, J.; Kanazawa, I.; Disteche, C. M.; Rubin, E. M.; Hayden, M. R. Human Huntingtin Derived from YAC Transgenes Compensates for Loss of Murine Huntingtin by Rescue of the Embryonic Lethal Phenotype. *Human Molecular Genetics* **1996**, *5* (12), 1875–1885. https://doi.org/10.1093/hmg/5.12.1875.

(57) Gauthier, L. R.; Charrin, B. C.; Borrell-Pagès, M.; Dompierre, J. P.; Rangone, H.; Cordelières, F. P.; de Mey, J.; MacDonald, M. E.; Leßmann, V.; Humbert, S.; Saudou, F. Huntingtin Controls Neurotrophic Support and Survival of Neurons by Enhancing BDNF Vesicular Transport along Microtubules. *Cell* **2004**, *118* (1), 127–138. https://doi.org/10.1016/j.cell.2004.06.018.

(58) Pal, A.; Severin, F.; Lommer, B.; Shevchenko, A.; Zerial, M. Huntingtin-HAP40 Complex Is a Novel Rab5 Effector That Regulates Early Endosome Motility and Is up-Regulated in Huntington's Disease. *Journal of Cell Biology* **2006**, *172* (4), 605–618. https://doi.org/10.1083/jcb.200509091.

(59) Feng, Z.; Jin, S.; Zupnick, A.; Hoh, J.; de Stanchina, E.; Lowe, S.; Prives, C.; Levine, A. J. P53 Tumor Suppressor Protein Regulates the Levels of Huntingtin Gene Expression. *Oncogene* **2006**, *25* (1), 1–7. https://doi.org/10.1038/sj.onc.1209021.

(60) Illuzzi, J. L.; Vickers, C. A.; Kmiec, E. B. Modifications of P53 and the DNA Damage Response in Cells Expressing Mutant Form of the Protein Huntingtin. *Journal of Molecular Neuroscience* **2011**, *45* (2), 256–268. https://doi.org/10.1007/s12031-011-9516-4.

(61) Munsie, L.; Caron, N.; Atwal, R. S.; Marsden, I.; Wild, E. J.; Bamburg, J. R.; Tabrizi, S. J.; Truant, R. Mutant Huntingtin Causes Defective Actin Remodeling during Stress: Defining a New Role for Transglutaminase 2 in Neurodegenerative Disease. *Human Molecular Genetics* **2011**, *20* (10), 1937–1951. https://doi.org/10.1093/hmg/ddr075.

(62) Steffan, J. S.; Kazantsev, A.; Spasic-Boskovic, O.; Greenwald, M.; Zhu, Y.-Z.; Gohler, H.; Wanker, E. E.; Bates, G. P.; Housman, D. E.; Thompson, L. M. The Huntington's Disease Protein Interacts with P53 and CREB-Binding Protein and Represses Transcription. *Proceedings of the National Academy of Sciences* **2000**, *97* (12), 6763–6768. https://doi.org/10.1073/PNAS.100110097.

(63) Benn, C. L.; Sun, T.; Sadri-Vakili, G.; McFarland, K. N.; DiRocco, D. P.; Yohrling, G. J.; Clark, T. W.; Bouzou, B.; Cha, J.-H. J. Huntingtin Modulates Transcription, Occupies Gene Promoters In Vivo, and Binds Directly to DNA in a Polyglutamine-Dependent Manner. *The Journal of Neuroscience* **2008**, *28* (42), 10720. https://doi.org/10.1523/JNEUROSCI.2126-08.2008.

(64) Cui, L.; Jeong, H.; Borovecki, F.; Parkhurst, C. N.; Tanese, N.; Krainc, D. Transcriptional Repression of PGC-1α by Mutant Huntingtin Leads to Mitochondrial Dysfunction and Neurodegeneration. *Cell* **2006**, *127* (1), 59–69. https://doi.org/10.1016/J.CELL.2006.09.015.

(65) Godin, J. D.; Colombo, K.; Molina-Calavita, M.; Keryer, G.; Zala, D.; Charrin, B. E. C.; Dietrich, P.; Volvert, M. L.; Guillemot, F.; Dragatsis, I.; Bellaiche, Y.; Saudou, F.; Nguyen, L.; Humbert, S. Huntingtin Is Required for Mitotic Spindle Orientation and Mammalian Neurogenesis. *Neuron* **2010**, *67* (3), 392–406. https://doi.org/10.1016/j.neuron.2010.06.027.

(66) Harding, R. J.; Deme, J. C.; Hevler, J. F.; Tamara, S.; Lemak, A.; Cantle, J. P.; Szewczyk, M. M.; Zuo, X.; Loppnau, P.; Seitova, A.; Fan, L.; Schapira, M.; Carroll, J. B.; R Heck, A. J.; Lea, S. M.; Arrowsmith, C. H. HAP40 Orchestrates Huntingtin Structure for 1 Differential Interaction with Polyglutamine 2 Expanded Exon 1. *bioRxiv* **2021**, 2021.04.02.438217. https://doi.org/10.1101/2021.04.02.438217.

(67) Harding, R. J.; Loppnau, P.; Ackloo, S.; Lemak, A.; Hutchinson, A.; Hunt, B.; Holehouse, A. S.; Ho, J. C.; Fan, L.; Toledo-Sherman, L.; Seitova, A.; Arrowsmith, C. H. A Toolkit of HTT Protein Resources 1 Design and Characterization of Mutant and Wild-Type Huntingtin Proteins Produced from a Toolkit of Scalable Eukaryotic Expression Systems A Toolkit of HTT Protein Resources 2 and the Tools Generated Here Lay a Foundation for Further Biochemical and Structural Work on the HTT Protein and for Studying Its Functional Interactions with Other Biomolecules. **2019**, *6*, 2020. https://doi.org/10.1074/jbc.RA118.007204.

(68) Levinson, B.; Kenwrick, S.; Lakich, D.; Hammonds, G.; Gitschier, J. A Transcribed Gene in an Intron of the Human Factor VIII Gene. *Genomics* **1990**, *7* (1), 1–11. https://doi.org/10.1016/0888-7543(90)90512-S.

(69) JA, N.; D, B.; P, G.; H, W.; D, B.; F, G. Investigation of the Factor VIII Intron 22 Repeated Region (Int22h) and the Associated Inversion Junctions. *Human molecular genetics* **1995**, *4* (7), 1217–1224. https://doi.org/10.1093/HMG/4.7.1217.

(70) BRASI, C. D. de; BOWEN, D. J. Molecular Characteristics of the Intron 22 Homologs of the Coagulation Factor VIII Gene: An Update. *Journal of Thrombosis and Haemostasis* **2008**, *6* (10), 1822–1824. https://doi.org/10.1111/J.1538-7836.2008.03094.X.

(71) Lakich, D.; Kazazian, H. H.; Antonarakis, S. E.; Gitschier, J. Inversions Disrupting the Factor VIII Gene Are a Common Cause of Severe Haemophilia A. **1993**.

(72) Williamson, J. INVESTIGATION OF THE HUNTINGTIN-HAP40 INTERACTION IN HUNTINGTON'S DISEASE, 2013.

(73) Seefelder, M.; Alva, V.; Huang, B.; Engler, T.; Baumeister, W.; Guo, Q.; Fernández-Busnadiego, R.; Lupas, A. N.; Kochanek, S. The Evolution of the Huntingtin-Associated Protein 40 (HAP40) in Conjunction with Huntingtin. *BMC Evolutionary Biology* **2020**, *20* (1), 162. https://doi.org/10.1186/s12862-020-01705-5.

(74) Pound, P.; Ritskes-Hoitinga, M. Is It Possible to Overcome Issues of External Validity in Preclinical Animal Research? Why Most Animal Models Are Bound to Fail. *Journal of Translational Medicine 2018 16:1* **2018**, *16* (1), 1–8. https://doi.org/10.1186/S12967-018-1678-1.

(75) Menalled, L. B.; Chesselet, M. F. Mouse Models of Huntington's Disease. *Trends in Pharmacological Sciences* **2002**, *23* (1), 32–39. https://doi.org/10.1016/S0165-6147(00)01884-8.

(76) Li, J. Y.; Popovic, N.; Brundin, P. The Use of the R6 Transgenic Mouse Models of Huntington's Disease in Attempts to Develop Novel Therapeutic Strategies. *NeuroRx* **2005**, *2* (3), 447. https://doi.org/10.1602/NEURORX.2.3.447.

(77) Slow, E. J.; Graham, R. K.; Osmand, A. P.; Devon, R. S.; Lu, G.; Deng, Y.; Pearson, J.; Vaid, K.; Bissada, N.; Wetzel, R.; Leavitt, B. R.; Hayden, M. R. Absence of Behavioral Abnormalities and Neurodegeneration in Vivo despite Widespread Neuronal Huntingtin Inclusions. **2005**, *102* (32).

(78) Gray, M.; Shirasaki, D. I.; Cepeda, C.; André, V. M.; Wilburn, B.; Lu, X.-H.; Tao, J.; Yamazaki, I.; Li, S.-H.; Sun, Y. E.; Li, X.-J.; Levine, M. S.; Yang, X. W. Full-Length Human Mutant Huntingtin with a Stable Polyglutamine Repeat Can Elicit Progressive and Selective Neuropathogenesis in BACHD Mice. *The Journal of Neuroscience* **2008**, *28* (24), 6182. https://doi.org/10.1523/JNEUROSCI.0857-08.2008.

(79) CP, M.; SE, H.; M, O.; KJ, K.; Y, Y.; KS, W.; MA, W.; WE, W.; JW, S. Absence of Cancer-Associated Changes in Human Fibroblasts Immortalized with Telomerase. *Nature genetics* **1999**, *21* (1), 115–118. https://doi.org/10.1038/5063.

(80) Mattis, V. B.; Svendsen, S. P.; Ebert, A.; Svendsen, C. N.; King, A. R.; Casale, M.; Winokur, S. T.; Batugedara, G.; Vawter, M.; Donovan, P. J.; Lock, L. F.; Thompson, L. M.; Zhu, Y.; Fossale, E.; Atwal, R. S.; Gillis, T.; Mysore, J.; Li, J. H.; Seong, I.; Shen, Y.; Chen, X.; Wheeler, V. C.; Macdonald, M. E.; Gusella, J. F.; Akimov, S.; Arbez, N.; Juopperi, T.; Ratovitski, T.; Chiang, J. H.; Kim, W. R.; Chighladze, E.; Watkin, E.; Zhong, C.; Makri, G.; Cole, R. N.; Margolis, R. L.; Song, H.; Ming, G.; Ross, C. A.; Kaye, J. A.; Daub, A.; Sharma, P.; Mason, A. R.; Finkbeiner, S.; Yu, J.; Thomson, J. A.; Rushton, D.; Brazier, S. P.; Battersby, A. A.; Redfern, A.; Tseng, H. E.; Harrison, A. W.; Kemp, P. J.; Allen, N. D.; Onorati, M.; Castiglioni, V.; Cattaneo, E.; Arjomand, J. Induced Pluripotent Stem Cells from Patients with Huntington's Disease Show CAG-Repeat-Expansion-Associated Phenotypes. *Cell Stem Cell* **2012**, *11* (2), 264–278. https://doi.org/10.1016/J.STEM.2012.04.027.

(81) Strehlow, A. N. T.; Li, J. Z.; Myers, R. M. Wild-Type Huntingtin Participates in Protein Trafficking between the Golgi and the Extracellular Space. *Human Molecular Genetics* **2007**, *16* (4), 391–409. https://doi.org/10.1093/HMG/DDL467.

(82) Truant, R.; Atwal, R. S.; Desmond, C.; Munsie, L.; Tran, T. Huntington's Disease: Revisiting the Aggregation Hypothesis in Polyglutamine Neurodegenerative Diseases. *FEBS Journal* **2008**, *275* (17), 4252–4262. https://doi.org/10.1111/j.1742-4658.2008.06561.x.

(83) Riguet, N.; Mahul-Mellier, A.-L.; Maharjan, N.; Burtscher, J.; Croisier, M.; Knott, G.; Hastings, J.; Patin, A.; Reiterer, V.; Farhan, H.; Nasarov, S.; Lashuel, H. A. Nuclear and Cytoplasmic Huntingtin Inclusions Exhibit Distinct Biochemical Composition, Interactome and Ultrastructural Properties. *bioRxiv* **2021**, 2020.07.29.226977. https://doi.org/10.1101/2020.07.29.226977.

(84) Shimogawa, M.; Petersson, E. J. New Strategies for Fluorescently Labeling Proteins in the Study of Amyloids. *Current Opinion in Chemical Biology* **2021**, *64*, 57–66. https://doi.org/10.1016/J.CBPA.2021.04.011.

(85) Bosch, P. J.; Corrêa, I. R.; Jr.; Sonntag, M. H.; Ibach, J.; Brunsveld, L.; Kanger, J. S.; Subramaniam, V. Evaluation of Fluorophores to Label SNAP-Tag Fused Proteins for Multicolor Single-Molecule Tracking Microscopy in Live Cells. *Biophysical Journal* **2014**, *107* (4), 803. https://doi.org/10.1016/J.BPJ.2014.06.040.

(86) Nikić, I.; Kang, J. H.; Girona, G. E.; Aramburu, I. V.; Lemke, E. A. Labeling Proteins on Live Mammalian Cells Using Click Chemistry. *Nature Protocols 2015 10:5* **2015**, *10* (5), 780–791. https://doi.org/10.1038/nprot.2015.045.

(87) Toseland, C. P. Fluorescent Labeling and Modification of Proteins. *Journal of Chemical Biology* **2013**, *6* (3), 85. https://doi.org/10.1007/S12154-013-0094-5.

(88) Marks, K. M.; Nolan, G. P. Chemical Labeling Strategies for Cell Biology. *Nature Methods 2006 3:8* **2006**, *3* (8), 591–596. https://doi.org/10.1038/nmeth906.

(89) Panchuk-Voloshina, N.; Haugland, R. P.; Bishop-Stewart, J.; Bhalgat, M. K.; Millard, P. J.; Mao, F.; Leung, W.-Y.; Haugland, R. P. Alexa Dyes, a Series of New Fluorescent Dyes That Yield Exceptionally Bright, Photostable Conjugates: *http://dx.doi.org/10.1177/002215549904700910* **2016**, *47* (9), 1179–1188. https://doi.org/10.1177/002215549904700910.

(90) Tabrizi, S. J.; Flower, M. D.; Ross, C. A.; Wild, E. J. Huntington Disease: New Insights into Molecular Pathogenesis and Therapeutic Opportunities. *Nature Reviews Neurology*. Nature Research October 1, 2020, pp 529–546. https://doi.org/10.1038/s41582-020-0389-4.

(91) Arrasate, M.; Finkbeiner, S. Protein Aggregates in Huntington's Disease. *Experimental Neurology*. NIH Public Access November 2012, pp 1–11. https://doi.org/10.1016/j.expneurol.2011.12.013.

(92) Rinaldi, C.; Wood, M. J. A. Antisense Oligonucleotides: The next Frontier for Treatment of Neurological Disorders. *Nature Reviews Neurology*. Nature Publishing Group January 1, 2018, pp 9–22. https://doi.org/10.1038/nrneurol.2017.148.

(93) *Wave Life Sciences Announces Topline Data and Addition of Higher Dose Cohort in Ongoing Phase 1b/2a PRECISION-HD2 Trial in Huntington's Disease*; 2019.

(94) Becanovic, K.; Nørremølle, A.; Neal, S. J.; Kay, C.; Collins, J. A.; Arenillas, D.; Lilja, T.; Gaudenzi, G.; Manoharan, S.; Doty, C. N.; Beck, J.; Lahiri, N.; Portales-Casamar, E.; Warby, S. C.; Connolly, C.; de Souza, R. A. G.; Tabrizi, S. J.; Hermanson, O.; Langbehn, D. R.; Hayden, M. R.; Wasserman, W. W.; Leavitt, B. R. A SNP in the HTT Promoter Alters NF-KB Binding and Is a Bidirectional Genetic Modifier of Huntington Disease. *Nature Neuroscience* **2015**, *18* (6), 807–816. https://doi.org/10.1038/nn.4014.

(95) Kingwell, K. Double Setback for ASO Trials in Huntington Disease. *Nature reviews. Drug discovery* **2021**, *20* (6), 412–413. https://doi.org/10.1038/D41573-021-00088-6.

(96) Roche - Roche provides update on tominersen programme in manifest Huntington's disease https://www.roche.com/media/releases/med-cor-2021-03-22b.htm (accessed 2021 -05 -03).

(97) palacino, james; swalley, susanne; song, C.; Cheung, atwood K.; shu, L.; Zhang, X.; van Hoosear, M.; shin, Y.; Chin, donovan; Gubser Keller, C.; Beibel, M.; renaud, nicole; smith, thomas M.; salcius, M.; shi, X.; Hild, M.; servais, rebecca; jain, M.; deng, L.; Bullock, C.; McLellan, M.; schuierer, sven; Murphy, L.; Blommers, M.; Blaustein, C.; Berenshteyn, F.; Lacoste, arnaud; thomas, jason; roma, G.; Michaud, G.; tseng, B.; porter, jeffery; Myer, V.; tallarico, john; Hamann, L. G.; Curtis, daniel; Fishman, M. C.; dietrich, W. F.; dales, natalie; sivasankaran, rajeev. SMN2 Splice Modulators Enhance U1–Pre-MRNA Association and Rescue SMA Mice. *nature CHeMICaL BIOLOGY* | **2015**, *11*. https://doi.org/10.1038/nCHeMBIO.1837.

(98) Sivasankaran, R. From Spinal Muscular Atrophy to Huntington's Disease Therapeutics. In *CHDI*; 2021.

(99) Carpenter, A. E.; Jones, T. R.; Lamprecht, M. R.; Clarke, C.; Kang, I. H.; Friman, O.; Guertin, D. A.; Chang, J. H.; Lindquist, R. A.; Moffat, J.; Golland, P.; Sabatini, D. M. CellProfiler: Image Analysis Software for Identifying and Quantifying Cell Phenotypes. *Genome Biology 2006 7:10* **2006**, *7* (10), 1–11. https://doi.org/10.1186/GB-2006-7-10-R100.

(100) Jares-Erijman, E. A.; Jovin, T. M. FRET Imaging. *Nature Biotechnology 2003 21:11* **2003**, *21* (11), 1387–1395. https://doi.org/10.1038/nbt896.

(101) Hochreiter, B.; Garcia, A. P.; Schmid, J. A. Fluorescent Proteins as Genetically Encoded FRET Biosensors in Life Sciences. *Sensors (Switzerland)* **2015**, *15* (10), 26281–26314. https://doi.org/10.3390/s151026281.

(102) Abraham, B. G.; Sarkisyan, K. S.; Mishin, A. S.; Santala, V.; Tkachenko, N. v.; Karp, M. Fluorescent Protein Based FRET Pairs with Improved Dynamic Range for Fluorescence Lifetime Measurements. *PLOS ONE* **2015**, *10* (8), e0134436. https://doi.org/10.1371/JOURNAL.PONE.0134436.

(103) Periasamy, A.; Mazumder, N.; Sun, Y.; Christopher, K. G.; Day, R. N. FRET Microscopy: Basics, Issues and Advantages of FLIM-FRET Imaging; Springer, Cham, 2015; pp 249–276. https://doi.org/10.1007/978-3-319-14929-5_7.

(104) Verveer, P. J.; Squire, A.; Bastiaens, P. I. H. Frequency-Domain Fluorescence Lifetime Imaging Microscopy: A Window on the Biochemical Landscape of the Cell. In *Methods in Cellular Imaging*; Springer New York: New York, NY, 2001; pp 273–294. https://doi.org/10.1007/978-1-4614-7513-2_16.

(105) Markwardt, M. L.; Kremers, G.-J.; Kraft, C. A.; Ray, K.; Cranfill, P. J. C.; Wilson, K. A.; Day, R. N.; Wachter, R. M.; Davidson, M. W.; Rizzo, M. A. An Improved Cerulean Fluorescent Protein with Enhanced Brightness and Reduced Reversible Photoswitching. *PLoS ONE* **2011**, *6* (3). https://doi.org/10.1371/JOURNAL.PONE.0017896.

(106) Banks, P. R.; Paquette, D. M. Comparison of Three Common Amine Reactive Fluorescent Probes Used for Conjugation to Biomolecules by Capillary Zone Electrophoresis. *Bioconjugate Chemistry* **2002**, *6* (4), 447–458. https://doi.org/10.1021/BC00034A015.

(107) Alex, A.; Piano, V.; Polley, S.; Stuiver, M.; Voss, S.; Ciossani, G.; Overlack, K.; Voss, B.; Wohlgemuth, S.; Petrovic, A.; Wu, Y.; Selenko, P.; Musacchio, A.; Maffini, S. Electroporated Recombinant Proteins as Tools for in Vivo Functional Complementation, Imaging and Chemical Biology. *eLife* **2019**, *8*. https://doi.org/10.7554/ELIFE.48287.

(108) Zhang, H.; Fan, J.; Wang, J.; Zhang, S.; Dou, B.; Peng, X. An Off-on COX-2-Specific Fluorescent Probe: Targeting the Golgi Apparatus of Cancer Cells. *Journal of the American Chemical Society* **2013**, *135* (31), 11663–11669. https://doi.org/10.1021/JA4056905.

(109) Shima, D. T.; Haldar, K.; Pepperkok, R.; Watson, R.; Warren, G. Partitioning of the Golgi Apparatus during Mitosis in Living HeLa Cells. *Journal of Cell Biology* **1997**, *137* (6), 1211–1228. https://doi.org/10.1083/JCB.137.6.1211.

(110) Xu, S.; Li, G.; Ye, X.; Chen, D.; Chen, Z.; Xu, Z.; Ye, L.; Stimming, E.; Marchionini, D.; Zhang, S. HAP40 Is a Conserved Central Regulator of Huntingtin and a Specific Modulator of Mutant Huntingtin Toxicity. *bioRxiv* **2020**, 2020.05.27.119552. https://doi.org/10.1101/2020.05.27.119552.

(111) Harding, R.; Deme, J.; Hevler, J.; Tamara, S.; Lemak, A.; Cantle, J.; Szewczyk, M.; Begeja, N.; Xiaobing, Z.; Loppnau, P.; Seitova, A.; Hutchinson, A.; Fan, L.; Truant, R.; Schapira, M.; Carroll, J.; Heck, A.; Lea, S.; Arrowsmith, C. Huntingtin Structure Is Orchestrated by HAP40 and Shows a Polyglutamine Expansion-Specific Interaction with Exon 1. *Communications Biology* **2021**.

(112) Tabrizi, S.; Leavitt, B.; Kordasiewicz, H.; Czech, C.; Swayze, E.; Norris, D. A.; Baumann, T.; Gerlach, I.; Schobel, S.; Smith, A.; Lane, R.; Bennett, C. F. Effects of IONIS-HTTRx in Patients with Early Huntington's Disease, Results of the First HTT-Lowering Drug Trial (CT.002). *Neurology* **2018**, *90* (15 Supplement).

(113) Sharma, A.; Singh, K.; Almasan, A. Histone H2AX Phosphorylation: A Marker for DNA Damage. *Methods in Molecular Biology* **2012**, *920*, 613–626. https://doi.org/10.1007/978-1-61779-998-3_40.

(114) Boeynaems, S.; Alberti, S.; Fawzi, N. L.; Mittag, T.; Polymenidou, M.; Rousseau, F.; Schymkowitz, J.; Shorter, J.; Wolozin, B.; Bosch, L. van den; Tompa, P.; Fuxreiter, M. Protein Phase Separation: A New Phase in Cell Biology. *Trends in Cell Biology* **2018**, *28* (6), 420–435. https://doi.org/10.1016/J.TCB.2018.02.004.

(115) Peters, M. F.; Ross, C. A. Isolation of a 40-KDa Huntingtin-Associated Protein *. *Journal of Biological Chemistry* **2001**, *276* (5), 3188–3194. https://doi.org/10.1074/JBC.M008099200.

(116) Kim, Y. J.; Yi, Y.; Sapp, E.; Wang, Y.; Cuiffo, B.; Kegel, K. B.; Qin, Z.-H.; Aronin, N.; DiFiglia, M. Caspase 3-Cleaved N-Terminal Fragments of Wild-Type and Mutant Huntingtin Are Present in Normal and Huntington's Disease Brains, Associate with Membranes, and Undergo Calpain-Dependent Proteolysis. *Proceedings of the National Academy of Sciences* **2001**, *98* (22), 12784–12789. https://doi.org/10.1073/PNAS.221451398.

(117) Mende-Mueller, L. M.; Toneff, T.; Hwang, S.-R.; Chesselet, M.-F.; Hook, V. Y. H. Tissue-Specific Proteolysis of Huntingtin (Htt) in Human Brain: Evidence of Enhanced Levels of N- and C-Terminal Htt Fragments in Huntington's Disease Striatum. *Journal of Neuroscience* **2001**, *21* (6), 1830–1837. https://doi.org/10.1523/JNEUROSCI.21-06-01830.2001.

(118) Demin, A. A.; Hirota, K.; Tsuda, M.; Hanzlikova, H.; Takeda, S.; Caldecott Correspondence, K. W. XRCC1 Prevents Toxic PARP1 Trapping during DNA Base Excision Repair. *Molecular Cell* **2021**, *81*, 3018–3030. https://doi.org/10.1016/j.molcel.2021.05.009.